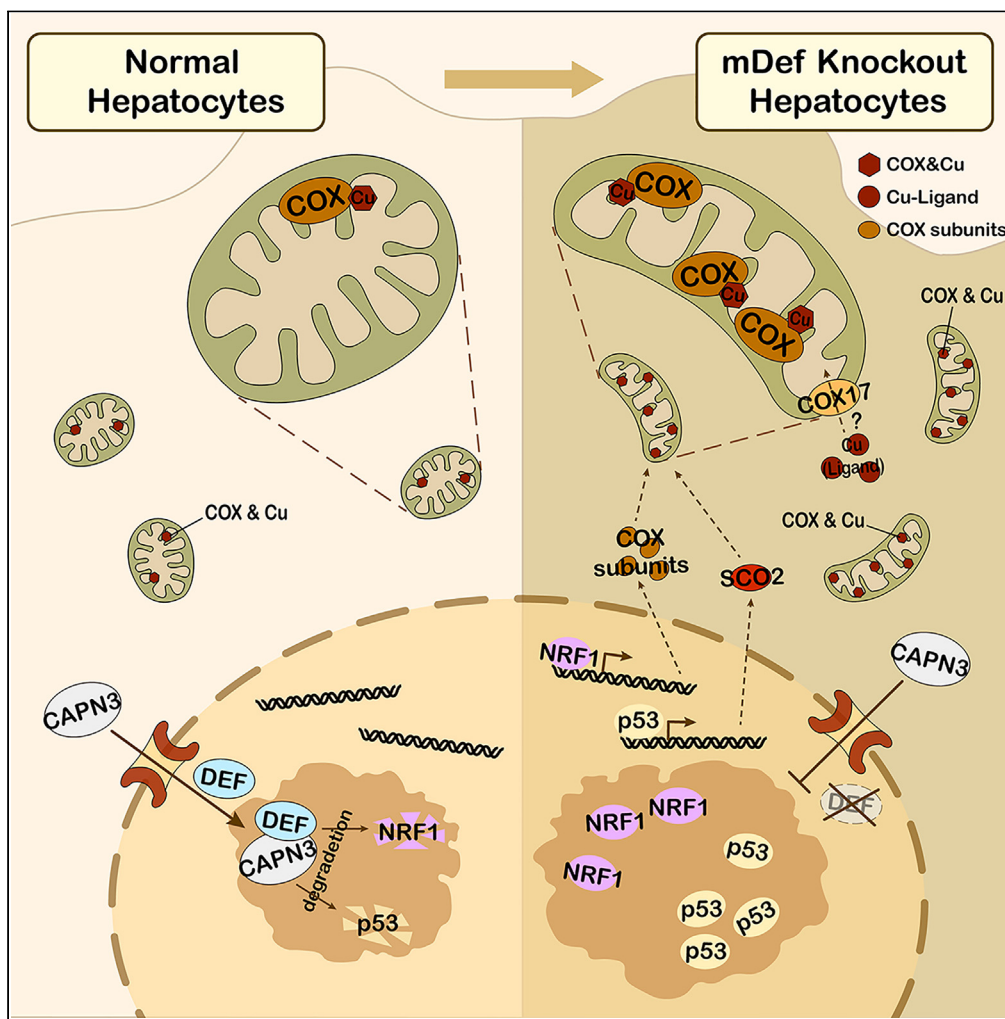


Article

Hepatic depletion of nucleolar protein mDEF causes excessive mitochondrial copper accumulation associated with p53 and NRF1 activation



Jinsong Wei,
Shuai Wang,
Haozhe Zhu, ...,
Bojing Liu, Jun
Chen, Jinrong
Peng

pengjr@zju.edu.cn

Highlights

Hepatic depletion of mDEF leads to Cu accumulation in mitochondria

Stabilized p53 in mDef-CKO upregulates Sco2 to promote mitochondria Cu uptake

Stabilized NRF1 in mDef-CKO upregulates Cox genes to promote mitochondrial Cu uptake

The mDEF-CAPN3 pathway regulates mitochondrial Cu homeostasis through p53 and NRF1

Figure360> For a Figure360 author presentation of this figure, see <https://doi.org/10.1016/j.isci.2023.107220>.

Wei et al., iScience 26, 107220
July 21, 2023 © 2023 The
Author(s).
<https://doi.org/10.1016/j.isci.2023.107220>



Article

Hepatic depletion of nucleolar protein mDEF causes excessive mitochondrial copper accumulation associated with p53 and NRF1 activation

Jinsong Wei,^{1,3} Shuai Wang,^{1,3} Haozhe Zhu,^{1,3} Wei Cui,¹ Jianan Gao,¹ Ce Gao,¹ Bo Yu,² Bojing Liu,¹ Jun Chen,² and Jinrong Peng^{1,4,*}

SUMMARY

Copper is an essential component in the mitochondrial respiratory chain complex IV (cytochrome *c* oxidases). However, whether any nucleolar factor(s) is(are) involved in regulating the mitochondrial copper homeostasis remains unclear. The nucleolar localized Def-Capn3 protein degradation pathway cleaves target proteins, including p53, in both zebrafish and human nucleoli. Here, we report that hepatic depletion of mDEF in mice causes an excessive copper accumulation in the mitochondria. We find that mDEF-depleted hepatocytes show an exclusion of CAPN3 from the nucleoli and accumulate p53 and NRF1 proteins in the nucleoli. Furthermore, we find that NRF1 is a CAPN3 substrate. Elevated p53 and NRF1 enhances the expression of *Sco2* and *Cox* genes, respectively, to allow more copper acquisition in the *mDef^{loxP/loxP}, Alb:Cre* mitochondria. Our findings reveal that the mDEF-CAPN3 pathway serves as a novel mechanism for regulating the mitochondrial copper homeostasis through targeting its substrates p53 and NRF1.

INTRODUCTION

Copper (Cu) homeostasis is vital to support the proper cellular functions in a healthy organism, and excess Cu loading is toxic to organisms.¹ For example, detrimental mutations in the *Atp7b* gene cause Wilson disease, which is clinically characterized by hepatic Cu accumulation and reduced ceruloplasmin (CP) activity in the serum.^{2,3} In mammals, Cu homeostasis is thought to be maintained by balancing the Cu absorption from the small intestine to the liver and Cu excretion to the bile duct. After being transported into the hepatocytes by the membrane transporter CTR1, Cu ions are bound with the Cu chaperone ATOX1 and are then transported to various subcellular organelles within the cell. When intracellular Cu concentration is excessive, ATOX1 delivers Cu to ATP7B, which is located in the trans-Golgi, and then ATP7B delivers Cu to CP, which can be excreted from hepatocytes by vesicular transport. *Atp7b*^{-/-} mutant mice liver exhibited a severe Cu overload.³⁻⁷

Cellular Cu homeostasis is especially important for mitochondria to exert their proper function because Cu is a central ion for superoxide dismutase (SOD) and cytochrome *c* oxidases (COX) in mammalian mitochondria.^{8,9} COX (i.e., mitochondrial respiratory chain complex IV) is an electron-driven proton pump involved in the final electron transport steps during mitochondrial respiration.¹⁰ Mammalian COX is a multimeric enzyme formed by 14 subunits of dual genetic origin: COX1, COX2, and COX3 are encoded by the mitochondrial DNA while others (COX4-1, COX5A, COX5B, COX6A1, COX6B1, COX6C, COX7A2, COX7B, COX7C, COX8-2, and NDUFA4) are encoded by the nuclear DNA.¹¹ Synthesis of cytochrome *c* oxidase 2 (SCO2) is a critical Cu chaperone responsible for transporting Cu from COX17 to COX II and assembling COX II subunit into the COX complex. Deficiency of SCO2 causes fatal encephalomyopathy because of aerobic respiratory failure.^{12,13} Studies have shown that *Sco2* transcription is directly activated by p53 and p53^{-/-} cells showed Cu deficiency.¹⁴ Nuclear respiratory factors 1 and 2 (NRF-1 and NRF-2) and the mitochondrial transcription factor A (TFAM) are the key transcriptional regulators of the *Cox* genes expression. TFAM controls the transcription of mitochondrial DNA encoded *Cox* genes while NRF-1 and NRF-2 are the primary transcription factors of nuclear DNA encoded *Cox* genes and also of *Tfam*.^{13,15} NRF-1 appears to be able to regulate all nuclear DNA encoded *Cox* components in neurons.¹⁶

¹MOE Key Laboratory for Molecular Animal Nutrition, College of Animal Sciences, Zhejiang University, Hangzhou 310058, China

²College of Life Sciences, Zhejiang University, Hangzhou 310058, China

³These authors contributed equally

⁴Lead contact

*Correspondence: pengjr@zju.edu.cn

<https://doi.org/10.1016/j.isci.2023.107220>



The *digestive organ expansion factor* (*def*, also called *utp25*) gene encodes a nucleolus-localized protein which serves as a member of the ribosome small subunit (SSU) assembly complex to regulate the processing of the 35S pre-rRNA in yeast or 47S in zebrafish and human to produce the mature 18S rRNA.^{17–20} In recent years, we have found that phosphorylated zebrafish Def can recruit the cysteine protease Calpain 3b (Capn3b)²¹ into the nucleolus to cleave target proteins harboring CAPN3-recognition sites.^{20,22–24} In the zebrafish *def* loss-of-function mutant (*def*^{hi429/hi429}), p53, a substrate of the Def-Capn3 pathway, accumulates in the nucleolus because of the lack of nucleolus-localized Capn3b which is associated with the hypoplastic digestive organ phenotype in the mutant embryos.^{19,25} We further showed that human p53 is also a CAPN3 target.^{19,23} In mice, genetic knockout of *mDef* caused embryonic lethality before implantation.^{26,27} Subsequent studies in mice with conditional knockout of *mDef* in the hepatocytes (*mDef*^{loxp/loxp}, *Alb:Cre*, designated as *mDef*-CKO thereafter) revealed that mouse livers developed pathological phenotypes such as immune cell infiltration, regional necrosis, bile duct over-proliferation, and enlarged nuclei. Meanwhile, male mutant mice died within 2–4 h after 70% hepatectomy, indicating that the function and homeostasis of the *mDef*-CKO liver was severely impaired.²⁷

In response to various cellular stresses, many proteins enter the nucleolus, either to be degraded or to form protein aggregates through the phase separation process.^{28–30} The Def-Capn3 protein cleavage pathway is proposed to be an important pathway for maintaining nucleolar protein homeostasis.²⁰ Herein, we carry out a detailed characterization of the *mDef*-CKO mice liver and find an excessive Cu accumulation in the mitochondria of the mDEF-depleted hepatocytes. Further investigation shows that NRF1, like p53, is a CAPN3 substrate and the mDEF-depletion results in the stabilization of p53 and NRF1 proteins in the nucleolus. The stabilized p53 and NRF1 promotes the expression of *Sco2* and *Cox* genes, respectively, which leads to a mitochondrial Cu accumulation. Pharmacological inhibition of p53 could partly rescue high Cu level caused by the mDEF depletion. Therefore, we unravel the molecular mechanism of maintaining intracellular and mitochondrial Cu homeostasis by the nucleolar localized DEF-CAPN3 protein degradation pathway.

RESULTS

Hepatic depletion of mDEF leads to Cu excessive accumulation in the liver

The *mDef*-CKO mice grew up normally with similar food intake as did the WT mice (Figure 1A), despite the fact that the mDEF protein level was drastically reduced in the *mDef*-CKO liver (Figure 1B). We noticed that while the WT liver was in pale color the *mDef*-CKO liver was brownish after lavage (Figure 1C), suggesting that there might be an accumulation of metal ions in the *mDef*-CKO liver. Detection of metal ions using the inductively coupled plasma mass spectrometry (ICP-MS) method showed that the Cu and iron (Fe) contents in the 3-month-old *mDef*-CKO liver were significantly higher than that in the WT liver whereas the light metal ion magnesium (Mg) remained at a similar level (Figure 1D). Ryanodine staining revealed that Cu was progressively accumulated from three to eight months in the *mDef*-CKO liver compared with that in the WT liver (Figure 1E).

Hepatic depletion of mDEF compromises the exporting rather than importing of Cu in the liver

Cu homeostasis in hepatocytes is regulated by the network formed by the importer CTR1, intracellular carrier ATP7B and chaperone ATOX1 and extracellular carrier Ceruloplasmin (CP).^{31–34} The qRT-PCR analysis³⁵ did not reveal a significant change in the mRNA levels of *Ctr1*, *Atp7b*, *Atox1*, and *Cp* in the *mDef*-CKO liver (Figure 2A). Consistently, except CTR1, the protein levels of ATP7B, ATOX1 and CP did not show an obvious change between the WT and *mDef*-CKO liver as detected by the western blot. The protein level of CTR1 was obviously elevated in the *mDef*-CKO liver (Figure 2B). CP is mainly produced by the liver and is then secreted to the serum. CP is an oxidative enzyme and 90% of the Cu in the plasma is bound by CP. A low CP enzyme activity in plasma indicates a liver Cu metabolism disorder.^{5,36} We determined the plasma CP enzyme activity using the enzyme activity assay kit and found that the CP activity in the *mDef*-CKO plasma was significantly lower than that in the WT plasma (Figure 2C). Using the ICP-MS method, we found that the Cu contents in both plasma and bile from the three-month-old *mDef*-CKO were significantly lower than that in the WT control (Figure 2D).

The above results suggest that the Cu exporting rather than absorption is probably compromised in the *mDef*-CKO hepatocytes. If this is the case, the extent of Cu accumulation in the *mDef*-CKO hepatocytes

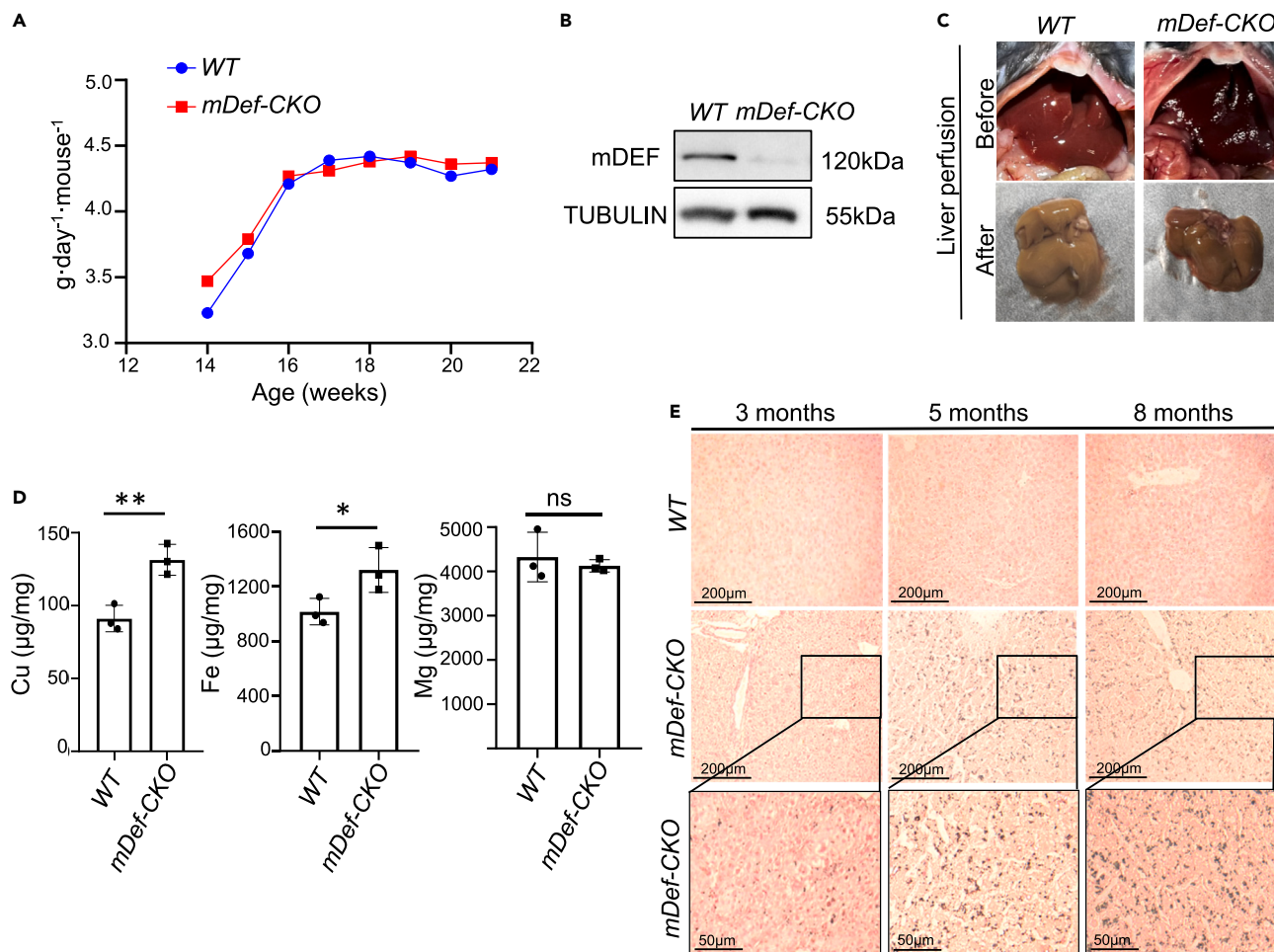


Figure 1. *mDef-CKO* mice accumulate Cu in the liver

(A) Average food intake recording for WT and *mDef-CKO* mice from 14 to 21 weeks postnatal (n = 3). WT and *mDef-CKO* male mice were raised in the same cage for recording.

(B) Western blot of the mDEF protein in the 3-month-old WT (*mDef^{flx/flx}*) and *mDef-CKO* liver. TUBULIN, loading control.

(C) Photo showing the liver color in a 3-month-old WT or *mDef-CKO* mouse before (upper panels) and after (lower panels) lavage.

(D) Detection of Cu, Fe and Mg in the 3-month-old WT and *mDef-CKO* liver using the ICP-MS method (n = 3). ns, no significance; *, p < 0.05; **, p < 0.01. Data are represented as mean ± SEM.

(E) Representative photos showing Ryanodine staining of the WT and *mDef-CKO* liver sections obtained from the 3-, 5- and 8-month-old mice (three mice examined for each stage), respectively. Magnified view of the boxed region the *mDef-CKO* liver section is provided.

could be correlated with dietary Cu. To verify this hypothesis, we performed a Cu chelator and Cu supplement feeding experiment, respectively.^{37,38} To exclude the early effect of the mDEF depletion caused by the *Alb:Cre*, we generated another *mDef* knockout model by tail vein injection of the AAV8:*TBG:Cre* virus to the 2-month-old *mDef^{loxP/loxP}* male mice (designated as *mDef-CKO^{AAV}*). Western blot analysis showed that mDEF protein almost undetectable in the *mDef-CKO^{AAV}* liver after two weeks of viral injection (Figure 2E). Male mice were divided into four groups, including the control groups of WT (i.e., *mDef^{loxP/loxP}*) and *mDef-CKO^{AAV}* fed with normal chow diet, and the experimental groups of *mDef-CKO^{AAV}* fed with normal chow diet supplemented with the Cu chelator DMSA or CuSO₄. The livers of these mice were dissected 60 days after the treatment (4-month-old) and were subjected to the ICP-MS analysis. For the normal chow diet fed control groups, the result confirmed the accumulation of Cu in the *mDef-CKO^{AAV}* liver when compared with the WT liver (Figure 2F). Of interest, the CuSO₄ supplement did not further enhance the Cu accumulation in the *mDef-CKO^{AAV}* liver (Figure 2F). On the other hand, the *mDef-CKO^{AAV}* mice fed with the Cu chelator supplement exhibited a significant reduction in the Cu accumulation (Figure 2F).

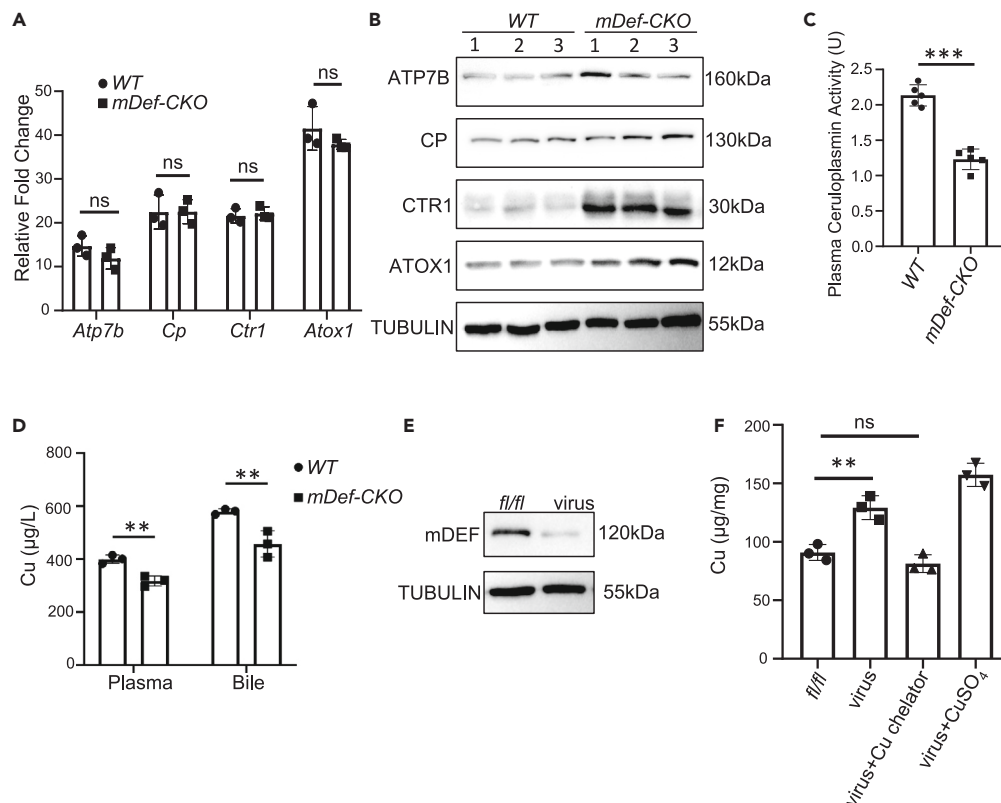


Figure 2. *mDef-CKO* hepatocytes are compromised in Cu exporting rather than importing

(A) qRT-PCR analysis of *Atp7b*, *Atox1*, *Cp* and *Ctr1* in the 3-months-old WT and *mDef-CKO* liver with three biological repeats. Expression level was expressed as relative fold change to the control gene *Actin*.
 (B) Western blot of ATP7B, CP, CTR1 and ATOX1 in three WT and three *mDef-CKO* mice livers (3-month-old). TUBULIN, loading control.
 (C) Comparing the plasma CP activity between 3-month-old WT and *mDef-CKO* mice (n = 5).
 (D) Detection of Cu contents in the plasma and bile from 3-month-old WT and *mDef-CKO* liver using the ICP-MS method (n = 3). ns, no significance; *, p < 0.05; **, p < 0.01.
 (E) Western blot of mDEF in the WT (*fl/fl*; *mDef^{flx/flx}*) and *mDef-CKO^{AAV}* liver. TUBULIN, loading control.
 (F) Detection of the liver Cu from the WT (*fl/fl*), *mDef-CKO^{AAV}* (virus), *mDef-CKO^{AAV}* administrated with Cu chelator (virus+Cu chelator) or CuSO₄ (virus+CuSO₄) male mice using ICP-MS (n = 3). ns, no significance; **, p < 0.01; ***, p < 0.001. Statistic data in A, C, D and F are represented as mean ± SEM.

Cu is excessively accumulated in the mitochondria in *mDef-CKO* hepatocytes

To determine the sub-cellular location of the Cu accumulation in the *mDef-CKO* hepatocytes, we performed a TEM analysis on the liver tissues from 3-month-old WT and *mDef-CKO* male mice, respectively. The result showed that a great proportion of the *mDef-CKO* nucleoli contained multiple white vacuoles (Figure S1A) and the sizes of the nucleoli of the mutant hepatocytes were significantly larger than that in WT (Figure S1B). Of interest, the mitochondria in the *mDef-CKO* hepatocytes exhibited a distorted and elongated morphology (Figures 3A, S2, and S3) together with a significant stronger electron density compared with the mitochondria in the WT hepatocytes (Figure 3B). In addition, based on analyzing the mt16S and mt12S rDNA versus genomic DNA ratio, we noticed that, in average, an *mDef-CKO* hepatocyte contained fewer number of mitochondria than did a WT hepatocyte (Figure 3C). To find out whether the enhanced electron density in the *mDef-CKO* mitochondria was related to an increase of the Cu content, we isolated the mitochondria from the WT and *mDef-CKO* hepatocytes by two steps of centrifugation (800 rpm and 15,000 rpm). ICP-MS analysis revealed that the Cu content was significantly higher in the *mDef-CKO* mitochondria than that in the WT mitochondria (Figure 3D). We then compared the Cu contents among the mitochondria, cytosol, and nuclei isolated from the WT and *mDef-CKO* hepatocytes, respectively (Figure S4A). The percentages of Cu contents in mitochondria, cytosol, and nuclei were approximately 44%, 20%, and 16% in WT, and 57%, 18%, and 14% in the *mDef-CKO*, respectively (Figure S4B),

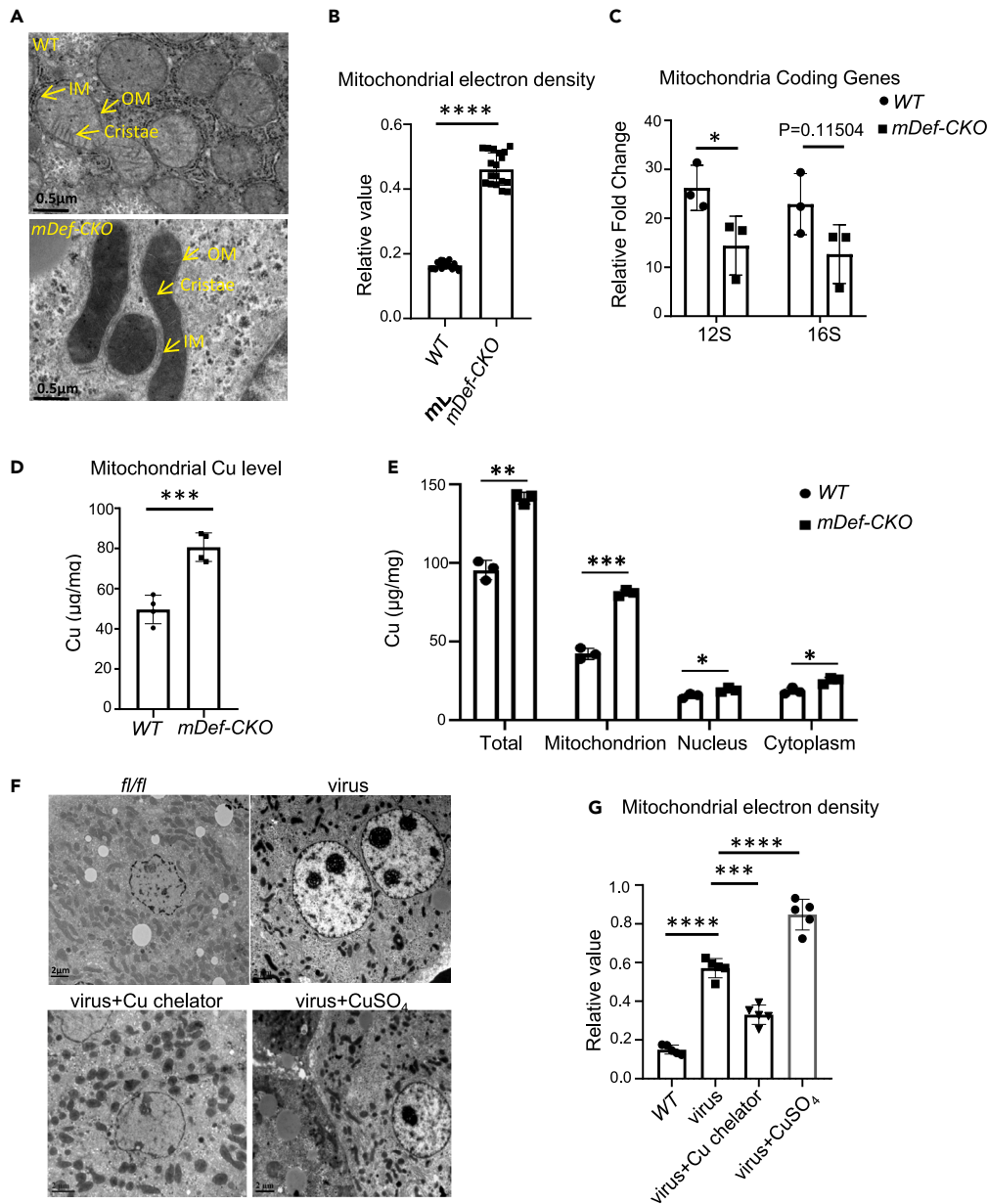


Figure 3. *mDef-CKO* hepatocytes accumulate Cu in the mitochondria

(A) Representative TEM images showing the mitochondria in the WT and *mDef-CKO* hepatocytes from 2-month-old mice (n = 3). Scale bar, 0.5 μ m. OM, outer membrane; IM, inner membrane. See also [Figures S2](#) and [S3](#).

(B) Statistical analysis of the electron density in WT and *mDef-CKO* mitochondria (n = 20) using the TEM images.

(C) Analysis of the mitochondria number in WT and *mDef-CKO* hepatocytes from three mice each based on comparing the ratio of 12S and 16S mitochondrial rDNA versus genomic DNA.

(D) Detection of Cu in the WT and *mDef-CKO* mitochondria using ICP-MS. The data was averaged from four biological repeats.

(E) Detection of Cu contents in the WT and *mDef-CKO* mitochondria, cytosol, and nuclei using ICP-MS. The data was averaged from three biological repeats.

(F) Representative TEM images comparing the morphology and mitochondrial electron density among the WT (*fl/fl*), *mDef-CKO*^{AAV} (virus), and *mDef-CKO*^{AAV} administrated with Cu chelator (virus+Cu chelator) or CuSO₄ (virus+CuSO₄) hepatocytes from 4-month-old mice. Scale bar, 2 μ m.

(G) Statistical analysis of the electron density in WT and *mDef-CKO*^{AAV} mitochondria based on the TEM images of five sections each. *, p < 0.05; ***, p < 0.001; ****, p < 0.0001. Statistic data in B-E and G are represented as mean \pm SEM.

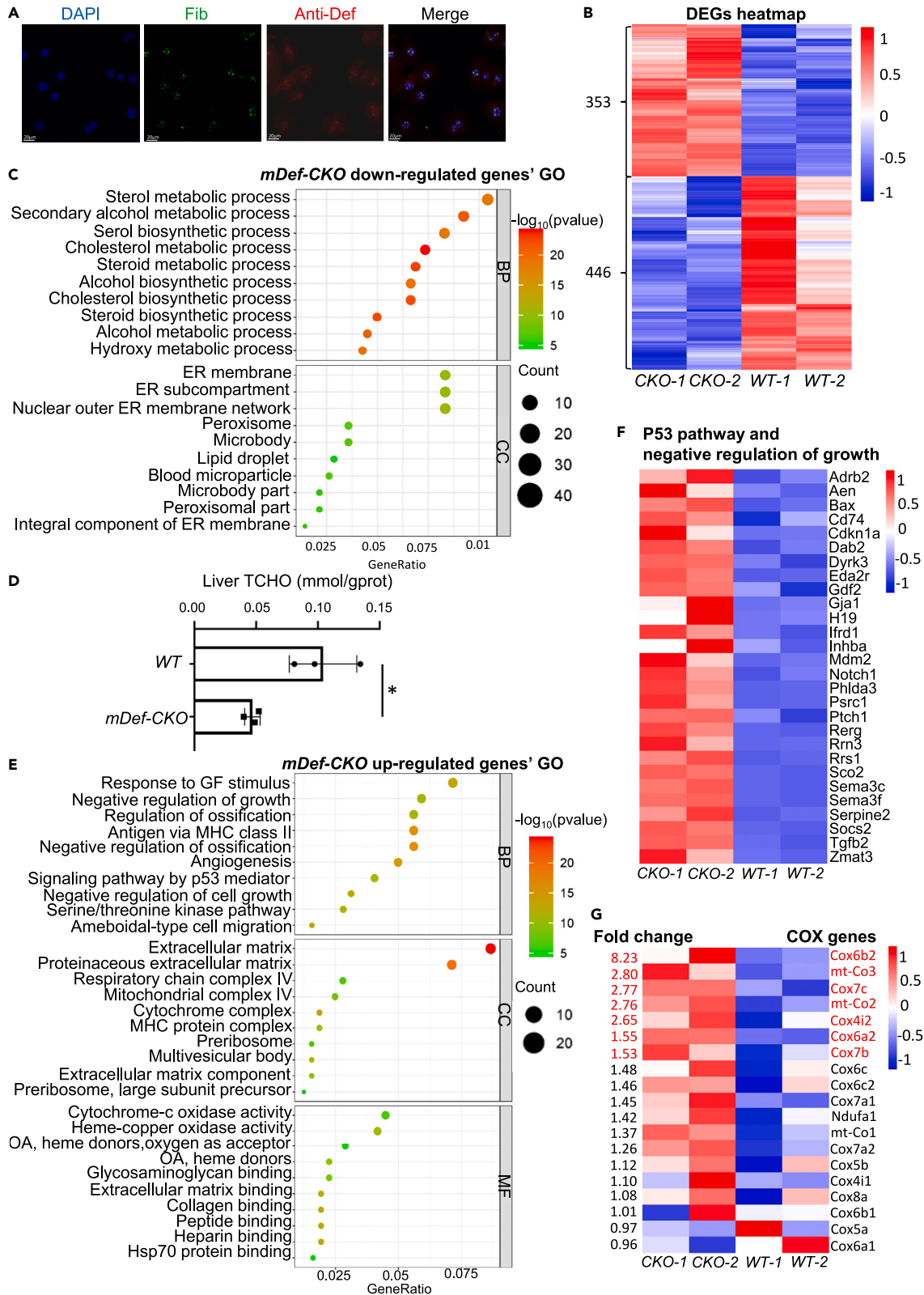


Figure 4. Bulk RNA-seq analysis reveals that mDEF depletion upregulates genes related to the p53 pathway and COX complex

- (A) Co-immunostaining of mDEF (red) and FIB (green) showing the nucleolar localization of mDEF. DAPI, staining the nuclei.
- (B) Heatmap showing the 446 downregulated and 353 upregulated DEGs identified from the RNA-seq data by comparing two WT and two *mDef*-CKO liver samples. See also [Tables S2](#) and [S3](#).
- (C) GO analysis of the 446 downregulated DEGs. Top 10 categories for the biological process (GO_BP) and cellular components (GO_CC) were shown, respectively. See also [Table S4](#).
- (D) Measurement of total cholesterol (TCHO) contents in the WT and *mDef*-CKO liver (n = 3). *, p < 0.05. Statistic data are represented as mean ± SEM.
- (E) GO analysis of the 353 upregulated DEGs. Top 10 categories for the GO_BP, GO_CC and molecular function (GO_MFs) were shown. See also [Table S5](#).
- (F) Heatmap showing 28 representatives upregulated DEGs related to the 'signaling pathway by p53 mediators' and 'negative regulation of growth' two categories under the GO_BP term.
- (G) Heatmap comparing the expression of all *Cox* genes in the WT and *mDef*-CKO liver. Genes with a fold-change (*mDef*-CKO vs. WT) > 1.5 are in red.

revealing a higher level of Cu in the mitochondria than in the cytosol and nuclei in both WT and *mDef*-CKO hepatocytes. With respect to the WT control, the *mDef*-CKO mitochondria exhibited a more significant increase in the Cu content than did the cytosol and nuclei ([Figure 3E](#)). These data suggest that Cu is probably preferentially accumulated in the mitochondria in the *mDef*-CKO hepatocytes.

In the Cu chelator DMSA and CuSO₄ supplement feeding model, the TEM analysis of *mDef*-CKO^{AAV} hepatocytes showed that while the mitochondrial electron density was significantly decreased by the Cu chelator it was enhanced by the CuSO₄ supplement ([Figures 3F](#) and [3G](#)), suggesting that the accumulated Cu contributed, at least partly, to the enhanced electron density in the *mDef*-CKO mitochondria. Meanwhile, the *mDef*-CKO^{AAV} mitochondria morphology appeared to be partially rescued by the Cu chelator supplement ([Figure 3F](#)). Together, these results suggested that the mDEF depletion in the hepatocytes altered the mitochondria morphology and led to an accumulation of Cu in the mitochondria.

Hepatic depletion of mDEF prominently activates the p53 pathway and upregulates the Cox genes

Immunostaining of mDEF in the cultured primary hepatocytes showed that, as the zebrafish *zDef* and human hDEF,^{19,23} mDEF was co-localized with the nucleolar marker protein Fibrillarin (FIB) ([Figure 4A](#)). Being a nucleolar protein, the depletion of mDEF causes a mitochondrial Cu accumulation but does not significantly alter the expression of genes related to the maintenance of the Cu homeostasis ([Figure 2A](#)), and this fact prompted us to investigate the molecular mechanism behind this phenotype. To this end, we performed a bulk RNA-seq analysis using liver tissues from 3-month-old WT and *mDef*-CKO mice, two mice for each genotype. Both hierarchical clustering ([Figure S5A](#)) and principal component analysis (PCA) ([Figure S5B](#)) showed that the two WT samples were closer to each other and so did the two *mDef*-CKO samples, suggesting that the bulk RNA-seq data were of satisfactory quality ([Table S1](#)). Compared with the averaged data from the WT samples, one *mDef*-CKO sample had 522 down- and 732 upregulated genes and another 668 down- and 1108 upregulated genes (fold-change <1.5 or >1.5, transcripts per million (TPM) > 1 in at least one sample, p < 0.05) ([Figure S5C](#)). The two *mDef*-CKO samples shared 237 downregulated and 389 upregulated genes ([Figure S5C](#)), a total of 626 differentially expressed genes (DEGs). When using the average data from the *mDef*-CKO samples for comparison, a total of 799 differentially expressed genes ([Figure S6A](#)), including 446 downregulated ([Table S2](#)) and 353 upregulated ([Table S3](#)) DEGs were identified in the *mDef*-CKO liver ([Figure 4B](#)). The 626 DEGs and 799 DEGs identified by the two different approaches shared 410 DEGs ([Figure S6B](#)), suggesting a high consistency between two analytic approaches. The 799 DEGs were subjected to the gene ontology (GO) analysis.

Of interest, data analysis based on TPM did not identify a significant difference in the *mDef* expression levels between the WT and *mDef*-CKO samples (fold-change = 0.41, p < 0.25) although the western blot analysis showed an obvious reduction in the mDEF protein in the *mDef*-CKO liver ([Figure 1B](#)). Further data analysis based on the Integrative Genomics Viewer (IGV) revealed that the conditional knockout of the *mDef* exon3 in *mDef*-CKO almost abolished the transcripts corresponding to the exon1, 2 and 3, however, the remaining exons (exon4-exon12) appeared to express at a level comparable to the WT ([Figure S6C](#)), suggesting that there might be an alternative transcription start site in the *mDef*-CKO liver. Consistent with the qRT-PCR analysis ([Figure 2A](#)), no significant difference was observed for the expression of *Ctr1*, *Atp7b*, *Atox1*, and *Cp*, the four genes related to the Cu homeostasis, between WT and *mDef*-CKO in the bulk RNA-seq data ([Figure S6D](#)).

GO analysis of the 446 downregulated DEGs under the 'biological process' (GO_BP) term showed that majority of the top 10 most significantly affected processes were related to the lipid metabolism, especially

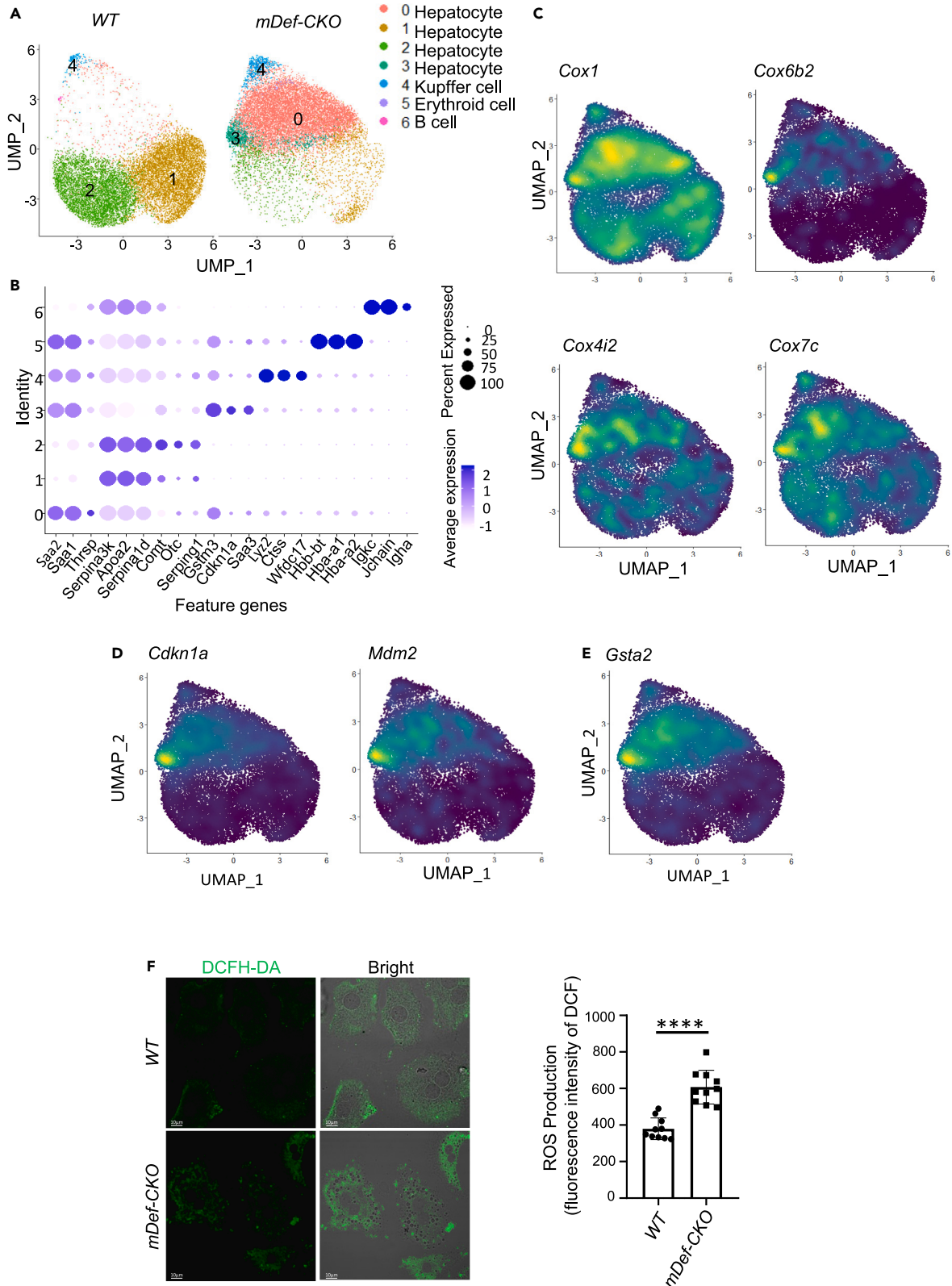


Figure 5. scRNA-seq analysis reveals an activation of the p53 pathway and increase of the oxidative stress in the *mDef-CKO* hepatocytes

(A) UMAP graphs comparing cell clusters between WT and *mDef-CKO*. Annotation of cell clusters is shown on the right.

(B) Dot plot showing three feature genes for each of the 7 cell clusters. See also [Table S7](#).

(C–E) Density map showing that the expression of *Cox1*, *Cox6b2*, *Cox4i2* and *Cox7c* (C), *Cdkn1a* (*p21*) and *Mdm2* (D) and *Gsta2* (E) genes were higher in cluster 0 and 3 hepatocytes.

(F) Images showing the fluorescence detection of ROS signals (left panels) and quantification of the ROS signal (using the ImageJ software package) (right panel) in WT and *mDef-CKO* hepatocytes. Statistic data are represented as mean \pm SEM.

sterol metabolic processes ([Figure 4C](#), [Table S4](#)). The genes involved included *Acs13*, *Acs15*, *Avpr1a*, *Ceacam*, *Dhcr7*, *Dhcr24*, *Gpld1*, *Hmgcr*, *Hmgcs1*, *Insig1*, *Mid1ip1*, *Msmo1*, *Mvd*, *Mvk*, *Nr1d1*, *Nsdhl*, *Ormdl2*, *Sc5d*, *Sqle*, *Sreb1*, and *Trib3* ([Figure S7](#), [Table S4](#)). Indeed, detection of total cholesterol (TCHO) in the liver showed that the level was significantly reduced in the *mDef-CKO* compared to the WT control ([Figure 4D](#)). This observation is consistent with previous reports showing that high Cu is associated with the dysregulation of sterol biosynthesis.^{39–41} Therefore, the function of the *mDef-CKO* liver appears to be compromised.

GO analysis of the 353 upregulated DEGs showed that three out of the top 10 most significantly affected GO_BPs were involved in the negative regulation of growth and signal pathway by p53 mediator ([Figure 4E](#)), including genes *Adrb2*, *Aen*, *Bax*, *Cd74*, *Cdkn1a*, *Dab2*, *Dyrk3*, *E2f2*, *Gja1*, *H19*, *Irf1*, *Inhba*, *Mdm2*, *Notch1*, *Phlda3*, *Pscc1*, *Rerg*, *Rrn3*, *Rrs1*, *Sema3c*, *Sema3f*, *Serpine2*, *Socs2*, *Tgfb2*, and *Zmat3* ([Figure 4F](#), [Table S5](#)). This result suggests that, as that observed in the zebrafish *def*^{-/-} mutant, the p53 signaling pathway is activated in the *mDef-CKO* liver. In addition, consistent with the observation of an invasion of immune cells in the *mDef-CKO* liver,²⁷ antigen via MHC class II process was also identified among the top 10 GO_BPs affected ([Figure 4E](#), [Table S4](#)).

Next, we examined the GO under the 'cellular component' (GO_CC) term for the 353 upregulated DEGs and found that, in addition to the 'extracellular matrix', 'MHC protein complex' and 'preribosome', three categories related to the mitochondria complex IV were among the top 10 GO_CC being affected ([Figure 4E](#)). Consistently, the COX activity was on the top of the top 10 categories identified using the 'molecular function' (GO_MF) term, including genes *mt-Co2* (*Cox2*), *mt-Co3* (*Cox3*), *Cox4i2*, *Cox6a2*, *Cox6b2*, *Cox7b* and *Cox7c* ([Figure 4G](#)).

scRNA-seq reveals malfunctioning hepatocytes in the *mDef-CKO* liver

To find out whether the upregulated DEGs related to the p53 pathway and mitochondrial respiratory chain complex IV happened in the *mDef-CKO* hepatocytes, we dissected the liver from WT and *mDef-CKO* male mice after perfusion and treatment with Collagenase IV. The purpose of the perfusion process was to remove the majority of blood cells in the liver, and that of the gentle Collagenase IV treatment was to keep the bile duct system undisrupted, in this way the dispersed cells for scRNA-seq were mainly hepatocytes. The obtained cells were subjected to an scRNA-seq analysis. Sequencing data from a total of 12295 and 13702 cells from the WT and *mDef-CKO* liver (one male mouse each), respectively, passed the quality control criteria ([Figures S8A](#), [S8B](#), and [Table S6](#)). Cell fractionation plots ([Figure S8C](#)) defined 7 cell clusters (cluster 0 to 6, dimensions 1:10, resolution 0.3) ([Figure 5A](#)). Annotation with feature genes ([Figure S9](#), [Table S7](#)) showed that cluster 4 represented the Kupffer cells ([Figure 5A](#)). Cluster 0 to 3 represented four subtypes of hepatocytes ([Figures 5A](#) and [5B](#)). The hepatocyte subtypes showed a drastic difference between WT and *mDef-CKO* samples, with WT containing mostly the cluster 1 and 2 hepatocytes while *mDef-CKO* mainly the cluster 0 and 3 ([Figure 5A](#)). The four subtypes of hepatocytes identified seemed not to match the hepatocytes defined by the three zones by examining the zonal markers *E-Cadherin* (*Cdh1*) (portal, zone 1), *Glutamine synthetase* (*Glu1*) (central, zone 3) and the proliferative marker *Mki67* in zone 2 (midzone).⁴² In WT, *Cdh1* and *Glu1* were expressed in both cluster 1 and 2 hepatocytes, despite expressing differentially in each individual cells ([Figure S10](#)). In contrast, these two genes were mainly expressed in cluster 0 and 3 cells in *mDef-CKO*, although with different expression level in each individual cells ([Figure S10](#)). Notably, *Mki67* was not detected in the WT hepatocytes but was obviously expressed in a fraction of cluster 3 hepatocytes in *mDef-CKO* ([Figure S10](#)), suggesting that some hepatocytes were likely undergoing renewing in the *mDef-CKO* liver.

Consistent with the bulk RNA-seq data analysis ([Figure 4F](#)), cluster 0 and 3 hepatocytes were characterized by high expression of *Cox1*, *Cox4i2*, *Cox6b2* and *Cox7c* ([Figure 5C](#)), a reflection of an elevated mitochondrial respiratory chain complex IV activity in *mDef-CKO*. In addition, Cluster 0 and 3 hepatocytes were

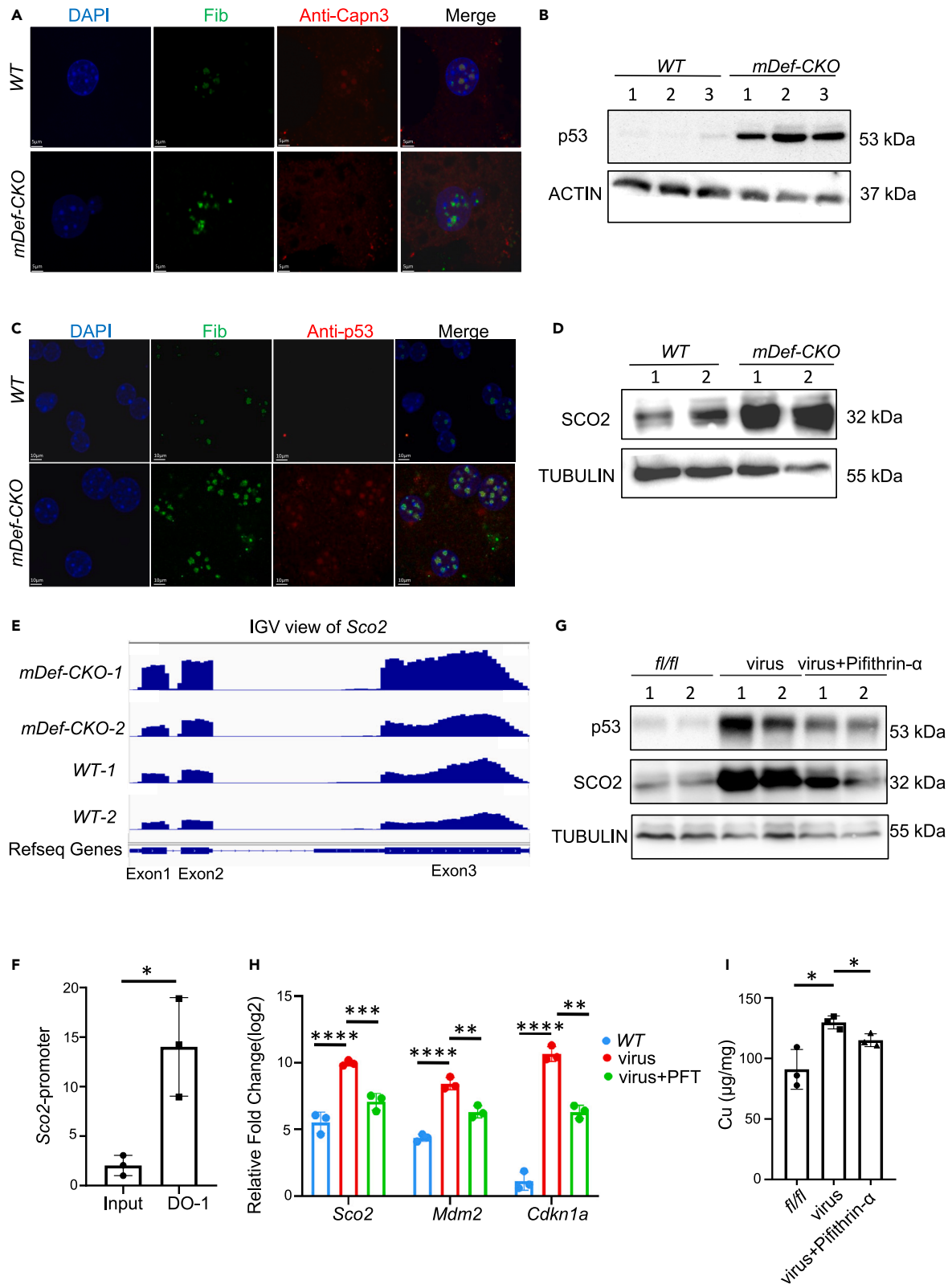


Figure 6. Elevated p53 in *mDef-CKO* hepatocytes promotes the expression of *Sco2* and p53 inhibitor PFT partially ameliorate the Cu accumulation in the *mDef-CKO*^{AAV}

- (A) Co-immunostaining of CAPN3 (red) and FIB (green) showing the exclusion of CAPN3 from the nucleolus in *mDef-CKO* hepatocytes. Scale bar, 5 μ m.
- (B) Western blot of p53 in the WT and *mDef-CKO* liver. ACTIN, loading control.
- (C) Co-immunostaining of p53 and FIB showing their co-localization in the nucleoli in the *mDef-CKO* hepatocytes. Scale bar, 10 μ m.
- (D) Western blot of SCO2 in the WT and *mDef-CKO* liver. TUBULIN, loading control.
- (E) IGV view of the *Sco2* transcripts detected by the RNA-seq in the WT and *mDef-CKO* liver.
- (F) ChIP-qPCR analysis of the enrichment of p53 on the *Sco2* promoter in the *mDef-CKO* liver. The ChIP product obtained by using the p53 antibody Do-1 was used for qRT-PCR using the *Sco2* promoter specific primers.
- (G) Western blot of p53 and SCO2 in the liver from the WT (*fl/fl*), *mDef-CKO*^{AAV} (virus) and *mDef-CKO*^{AAV} mice administrated with the p53 inhibitor PFT (virus+PFT). TUBULIN, loading control.
- (H) qRT-PCR analysis of *Cdkn1a*, *Mdm2* and *Sco2* in the *mDef-CKO*^{AAV} liver after the injection of PFT. Expression level was normalized against *Actin*.
- (I) Measurement of the Cu content in the WT, *mDef-CKO*^{AAV}, and *mDef-CKO*^{AAV} liver injected with PFT using ICP-MS. Statistic data in F, H and I are represented as mean \pm SEM.

characterized by high expression of *Cdkn1a* and *Mdm2* (Figure 5D), suggesting an activation of the p53 pathway in *mDef-CKO*. Strikingly, *Gsta2*, a gene responding to high intracellular level of oxidative stress,⁴³ was expressed at a high level in Cluster 0 and 3 hepatocytes (Figure 5E). Fluorescence staining using the ROS substrate DCFH-DA (Figure 5F, left panels) and quantification of the staining signals using ImageJ (Figure 5F, right panel) showed that the ROS level was indeed increased in *mDef-CKO* hepatocytes. The scRNA-seq data suggest that the *mDef-CKO* hepatocytes suffered from the oxidative stress which might be the consequence of the activation of the p53 pathway and elevation of the COX activity.^{44,45}

Hepatic depletion of mDEF leads p53 to be accumulated in the nucleolus

Although the p53 pathway is activated in the *mDef-CKO* hepatocytes, checking the RNA-seq data did not reveal an elevation of the p53 transcript level in the mutant liver (Figure S11A). We have previously reported that p53 is a CAPN3 substrate, and that depletion of zebrafish *zDef* or knockdown of human *hDEF* causes the exclusion of *Capn3b*/CAPN3 from the nucleolus that results in accumulation of p53 in the nucleolus.^{19,23} To find out whether this is the case for mDEF, we performed a co-immunostaining of FIB and CAPN3 in the cultured WT and *mDef-CKO* primary hepatocytes. The cultured *mDef-CKO* primary hepatocytes lacked a detectable mDEF (Figure S11B). The co-immunostaining result showed that while FIB and CAPN3 were co-localized in the nucleolus in the WT hepatocytes CAPN3 appeared to be excluded from the nucleolus in the *Def-CKO* hepatocytes (Figure 6A). Consequently, the p53 protein level was significantly increased in the *mDef-CKO* mice liver (Figure 6B). Immunostaining of hepatocytes primary cells showed that the elevated p53 is colocalized with the FIB in the nucleoli of the *mDef-CKO* hepatocytes (Figure 6C). Of interest, a TUNEL assay on the liver section did not reveal any significant difference in apoptotic cells between WT and *mDef-CKO* (Figure S11C).

Elevated p53 promotes the hepatic *Sco2* expression and Cu accumulation

As an important transcription factor, p53 regulates cellular metabolism and mitochondrial respiration,^{44,45} one way is through regulating the expression of its target gene *Synthesis of cytochrome c oxidase 2* (*Sco2*). *Sco2* is a nuclear gene and encodes SCO2 which serves as a critical Cu chaperone for assembling the COX in mitochondria. p53 can bind to the *Sco2* promoter to activate the *Sco2* expression.⁴⁴ Mutations in *Sco2* greatly reduce the Cu level in cells.^{14,46,47}

Examination of SCO2 revealed a marked increase in its protein level in the *mDef-CKO* liver compared with the WT (Figure 6D). In contrast, the Cu chaperone for superoxide dismutase (CCS) protein level did not show a significantly change (Figure S11D). Checking the bulk RNA-seq data showed that the *Sco2* transcript level was elevated in *mDef-CKO* (Figure 6E). We then performed a ChIP-qPCR analysis using the ChIP product pulled down by a p53-specific antibody (DO-1) and found that p53 was enriched in the promoter region of *Sco2* in the *mDef-CKO* liver (Figure 6F).

To explore the direct role of p53 on Cu accumulation, we performed a rescue experiment by the injection of PFT, a p53 inhibitor.⁴⁸ Male mice were divided into three groups: *mDef*^{*loxP/loxP*} control, *mDef-CKO*^{AAV} control, and *mDef-CKO*^{AAV} injected with PFT (inject once every two days for a duration of 45 days). Western blot analysis showed that p53 protein is accumulated in the *mDef-CKO*^{AAV} group but this increase was downregulated by PFT (Figure 6G). The effectiveness of PFT was confirmed by its negative effect on the expression of the p53 target genes *Cdkn1a* and *Mdm2* (Figure 6H). Injection of PFT obviously reduced

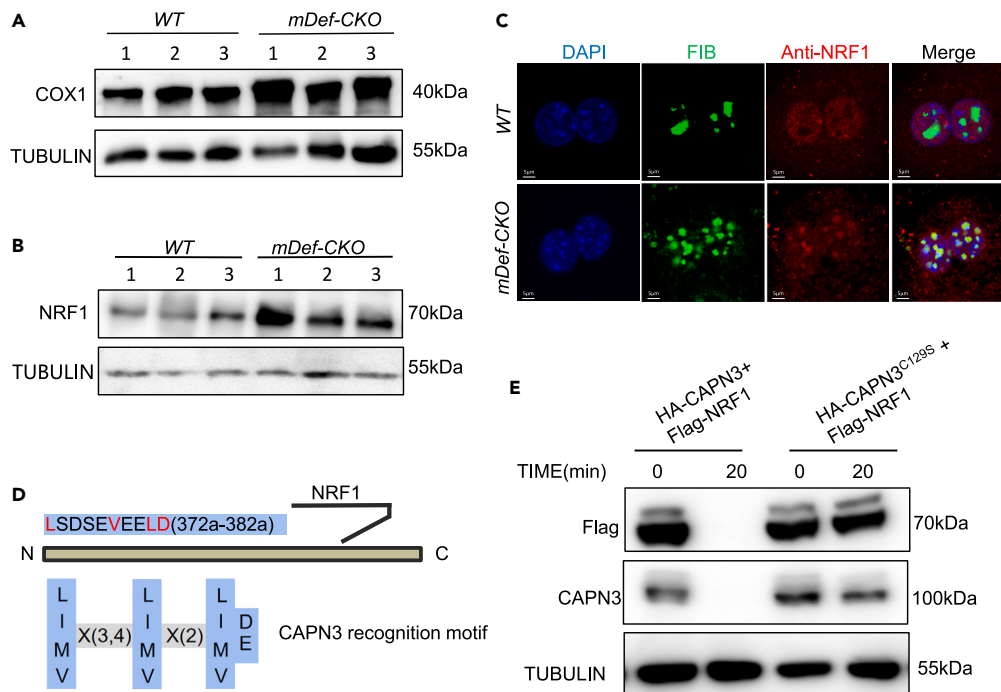


Figure 7. NRF1 is stabilized in the *mDef-CKO* hepatocytes and is a CAPN3 substrate

(A and B) Western blot of COX1 (A) and NRF1 (B) in the livers from three WT and three *mDef-CKO* male mice. TUBULIN, loading control.

(C) Co-immunostaining of NRF1 (red) and FIB (green) in the WT and *mDef-CKO* hepatocytes. DAPI, staining the nuclei.

(D) Diagram showing the CAPN3 recognition site in NRF1. The key amino acids in NRF1 for CAPN3 recognition are in red letters. Low panel, CAPN3 recognition motif.

(E) Western blot of NRF1 and CAPN3 showing that NRF1 is a CAPN3 substrate.

both the hepatic *Sco2* transcript and SCO2 protein levels in *mDef-CKO^{AAV}* (Figures 6G and 6H). Comparing the liver Cu contents in the above three groups of mice using ICP-MS showed that PFT could partially ameliorate the Cu accumulation in *mDef-CKO^{AAV}* (Figure 6F).

NRF1 is a CAPN3 substrate and is enriched in the nucleolus by mDEF depletion

To find out whether the upregulation of the *Cox* genes would lead to an increase in the mitochondrial respiratory chain complex IV in the *mDef-CKO* liver, we performed a western blot analysis. The result showed that COX1 was significantly increased in the *mDef-CKO* liver (Figure 7A). Because the number of mitochondrial slightly decreased in the *mDef-CKO* hepatocytes, this observation indicated that the *mDef-CKO* mitochondria had more COX complex, which nicely correlates with the Cu accumulation in the *mDef-CKO* mitochondria.

Previous studies have shown that the transcription of the nuclear coded *Cox* subunits is regulated by NRF-1 and NRF-2.¹⁶ The fact that the transcript levels of the nuclear encoded *Cox4i2*, *Cox6a2*, *Cox6b2*, *Cox7b* and *Cox7c* were upregulates in the *mDef-CKO* liver (Figure 4F) suggested an upregulation of NRF1 or NRF2. Surprisingly, checking the bulk RNA-seq data did not reveal an upregulation of the *Nrf1* or *Nrf2* transcripts (Figure S6D), suggesting that NRF1 or NRF2 protein was stabilized in the *mDef-CKO* hepatocytes. Indeed, western blot analysis showed that NRF1 was significantly increased in the mutant liver (Figure 7B). Co-immunostaining of NRF1 and FIB showed that the elevated NRF1 was localized in the nucleolus in the *mDef-CKO* hepatocytes (Figure 7C).

We wondered whether NRF1 or NRF2 is a target of the DEF-CAPN3 pathway and the accumulation of NRF1 or NRF2 in the *mDef-CKO* nucleoli might be because of the exclusion of CAPN3 from the nucleolus. To test this hypothesis, we checked whether NRF1 or NRF2 harbors a putative CAPN3-recognition site^{21,23} and found that NRF1 but not NRF2 has a recognition site (Figure 7D). Next, we expressed human CAPN3,

CAPN3^{C129S} (an inactive form of CAPN3 because of the substitution of C¹²⁹ by S¹²⁹ at the activity center) and mouse NRF1, respectively, in 293T cells. The expressed CAPN3 and CAPN3^{C129S} were extracted from the cultured cells and then mixed with the NRF1 protein extract, respectively. The mixture was incubated at 37°C for 20 min before being subjected to western blot analysis. The result showed that the CAPN3 protein extract but not the CAPN3^{C129S} extract greatly reduced the NRF1 protein level (Figure 7E), demonstrating that NRF1 is a CAPN3 substrate.

Mitochondria Cu transporter COX17 is upregulated in the *mDef*-CKO liver

COX17 is a chaperone protein that transports Cu from the cytosol to the mitochondria and then deliver Cu to SCO1/2 while SCO2 is responsible for delivering the Cu to the copper A (CuA) site of COX2.^{8,49} Checking our RNA-seq data did not find a significant change in *Cox17* transcript levels between WT and *mDef*-CKO (Figure S6D). However, the western blot analysis revealed an obvious elevation of the COX17 protein level in the *mDef*-CKO liver (Figure 8A). Checking the expression of *Slc25a3*, which encodes another mitochondria Cu transporter SLC25A3, in our RNA-seq data we found that *Slc25a3* was slightly but not significantly upregulated (fold change = 1.24, p = 0.11). We reexamined the *Slc25a3* expression level by qPCR and found that *Slc25a3* was slightly but significantly upregulated in the *mDef*-CKO liver (Figure 8B). Considering the observation that Cu was more prominently accumulated in mitochondria than in the cytosol and nuclei (Figure 3E), these data suggest that Cu is probably preferentially transported to the mitochondria through the COX17-SCO2 pathway in the *mDef*-CKO liver.

DISCUSSION

Cu is a trace element, essential for neurotransmitter, neuropeptide and collagen biosynthesis, wound healing, angiogenesis, growth and iron utilization.³¹ Importantly, Cu is a cofactor for the COX complex and intracellular Cu deficiency may cause mitochondrial dysfunction. Conversely, mitochondrial Cu overload can enhance aerobic respiration and increase ROS level.^{10,11} In hepatocytes, the Cu homeostasis is maintained by multiple factors such as CTR1, ATOX1, ATP7B and CP which regulate the balance of importing and exporting. On the other hand, PIC2 and SLC25A3 are responsible for transporting Cu to the mitochondria for assembling the COX complex.^{50,51} Here, we report the finding of an unexpected role of the nucleolar localized DEF-CAPN3 pathway in regulating the COX complex. We show that hepatic depletion of mDEF causes the stabilization of p53 and NRF1 which then promotes the expression of *Sco2* and *Cox* genes, respectively, which finally leads to the Cu accumulation in the mitochondria and alters the morphology of the mitochondria (Figure 8C).

The mouse genome contains only one copy of *mDef* and the early lethality of the *mDef*-knockout mice suggests the importance of mDEF for cellular activities and cell survival.^{26,27} This might explain the observation that the *mDef*-CKO hepatocytes were morphologically deformed and expressed different features genes as revealed by TEM and scRNA-seq, respectively. Previous studies have shown that DEF/UTP25 not only serves as a component of the SSU processome¹⁸ but also functions to recruit CAPN3 to the nucleolus to cleave target proteins such as p53 and Mpp10.^{19,52} Indeed, as that observed in zebrafish, the p53 protein level was obviously increased and was accumulated in the *mDef*-CKO nucleolus. The p53 protein level must be kept at a low level by Mdm2 and other E3 ligases in a normal cell because, as a transcription factor, an elevated p53 activity promotes cell-cycle arrest and cell apoptosis and alters mitochondrial activities. p53 regulates the mitochondrial activity through its target gene *Sco2*.^{44,45} Our RNA-seq analysis revealed *Sco2* was among the upregulated DEGs. SCO2 is part of the COX holo-enzymes and is required for transfer of Cu from COX17 to the COX complex. Therefore, we establish an axis that couples the nucleolar mDEF-CAPN3 pathway with the p53-SCO2 pathway for regulating the mitochondrial Cu homeostasis.

It is exciting to find that NRF1 is a target of CAPN3 and NRF1 is accumulated in the *mDef*-CKO nucleolus. This finding nicely explains the upregulation of multiple genes encoding the members of the COX complex. The increase in the level of the COX complex in the *mDef*-CKO mitochondria is consistent with the observation of the Cu accumulation in the mitochondria because Cu is an important cofactor in the COX complex. These results suggest that, in addition to the regulation of the p53 pathway, the nucleolar mDEF-CAPN3 pathway also operates through NRF1 to regulate the mitochondrial function.

The RNA-seq data did not reveal a significant alteration in the expression of genes involved in the cellular Cu importing and exporting, including *Ctr1*, *Atox1*, *Atp7b* and *Cp*, suggesting that the mDEF-CAPN3 pathway might not participate in the regulation of these genes. Consistently, the protein levels of

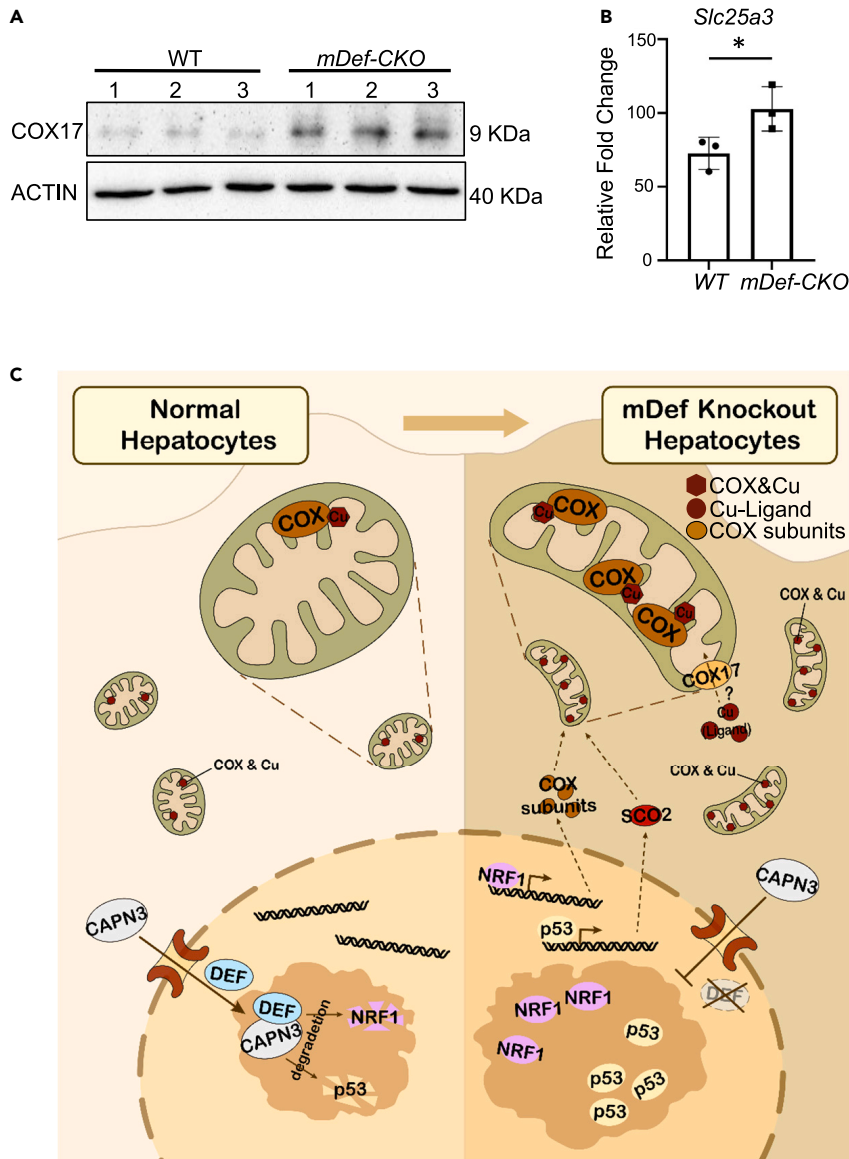


Figure 8. The nucleolar mDEF-CAPN3 pathway regulates the mitochondrial Cu homeostasis through p53 and NRF1

(A) Western blot of COX17 in WT and *mDef*-CKO liver. ACTIN, loading control.

(B) qPCR analysis of *Slc25a3* transcript levels in WT and *mDef*-CKO liver. Relative expression fold change against β -Actin was shown. Statistic data are represented as mean \pm SEM.

(C) A model illustrates the role of the nucleolar mDEF-CAPN3 pathway in regulating the mitochondrial activity through p53 and NRF1. Exclusion of CAPN3 from the nucleolus because of mDEF depletion activates the p53 pathway for *SCO2* expression and the NRF1 pathway for the *Cox* genes expression which finally leads to an excessive Cu accumulation in hepatocytes.

ATOX1, ATP7B and CP were not obviously altered in the *mDef*-CKO liver. However, we noticed that the CTR1 protein level is elevated and the reason is currently unknown. Probably because of an elevated activity of SCO2 and the COX complex,⁵³ we detected an increase of ROS level in *mDef*-CKO hepatocytes, suggesting a detrimental outcome of the elevated COX activity. Of interest, TUNEL assay did not reveal an elevated apoptotic activity in the *mDef*-CKO liver and the deformed mitochondria was able to be preserved. Our RNA-seq data also revealed that the cholesterol metabolic pathway was the most significantly affected biological process in the *mDef*-CKO liver. Of interest, previous transcriptomic analysis revealed that cholesterol biosynthesis appeared to be the most significantly affected process in the *Atp7b*-deficient

mice, causing ~30% reduction of total cholesterol in the liver.^{39,40} In addition, it was found that broiler fed with Cu-supplement exhibited a reduction in total liver cholesterol which might related to the downregulation of SREBP2 expression.⁴¹ Therefore, the accumulated Cu in the *mDef*-CKO liver might be the reason for the dysregulation of cholesterol biosynthesis, however, we cannot exclude the possibility that the other defects caused mDEF-deficiency might contribute to this observation.

In summary, here, we unravel a novel molecular mechanism which regulates the mitochondrial function by the nucleolar mDEF-CAPN3 protein degradation pathway through targeting p53 and NRF1. Malfunctioning of this pathway leads to Cu accumulation in the mitochondria. It would be interesting to study whether there is a correlation between the DEF-CAPN3 pathway and Wilson disease in the future. One report showed that the expression of human *DEF* (*hDEF*) in cultured HepG2 cells was upregulated by either ATP7B knockdown or Cu supplement.⁵⁴ This data together with our findings suggest that DEF might function to protect cells by blocking Cu accumulation, however, more evidences are needed to verify this hypothesis.

LIMITATION OF THE STUDY

In this study, we showed that mDEF-depleted hepatocytes accumulated Cu in the mitochondria which was associated with the nucleolar enrichment of p53 and NRF1 since these two transcription factors regulate the expression of *Sco2* and *Cox* genes, respectively. However, whether the Cu accumulation resulted from mDEF-depletion has any correlation with that observed in the Wilson disease patients remains elusive. In addition, how the Cu-exporting is affected in the mDEF-depleted hepatocytes needs further investigation.

STAR★METHODS

Detailed methods are provided in the online version of this paper and include the following:

- KEY RESOURCES TABLE
- RESOURCE AVAILABILITY
 - Lead contact
 - Materials availability
 - Data and code availability
- EXPERIMENTAL MODEL AND STUDY PARTICIPANT DETAILS
 - Mouse stains
- METHOD DETAILS
 - Ryanodine staining
 - Drug treatment
 - Transmission electron microscopy (TEM)
 - Liver tissue harvesting and primary hepatocyte culture
 - Mitochondria isolation
 - Protein analysis
 - Quantitative real-time PCR (qRT-PCR)
 - Bulk RNA-seq
 - Single cell RNA sequencing (scRNA-seq)
 - Immunofluorescence staining
 - Nuclei isolation
 - Bile collection
 - Liver total cholesterol detection
- QUANTIFICATION AND STATISTICAL ANALYSIS
 - Hepatic Cu quantification
 - Differential gene-expression analysis of RNA sequencing data
 - scRNA-seq data analysis
 - Detection of intracellular ROS
 - Statistical analysis

SUPPLEMENTAL INFORMATION

Supplemental information can be found online at <https://doi.org/10.1016/j.isci.2023.107220>.

ACKNOWLEDGMENTS

We thank all other members in JRP and JC lab for their valuable suggestions. This work is supported by the National Natural Science Foundation of China (U21A20198) and the National Key R&D Program of China (2018YFA0800502).

AUTHOR CONTRIBUTIONS

Conceptualization, J.S.W., S.W., Z.H.Z., and J.R.P.; methodology, J.S.W., S.W., C.G., B.J.L., and J.C.; formal analysis, S.W., and Z.H.Z.; investigation, J.S.W., S.W., Z.H.Z., W.C., J.N.G., B.Y., C.G., and B.J.L.; resources, C.G., B.J.L., and J.R.P.; writing – original draft, J.S.W., S.W., Z.H.Z., and J.R.P.; writing – reviewing and editing, all authors; supervision, C.G., J.C., and J.R.P.; funding acquisition, J.R.P.

DECLARATION OF INTERESTS

The authors declare no competing interests.

Received: March 3, 2023

Revised: May 15, 2023

Accepted: June 22, 2023

Published: June 26, 2023

REFERENCES

- Aggarwal, A., and Bhatt, M. (2020). Wilson disease. *Curr. Opin. Neurol.* 33, 534–542. <https://doi.org/10.1097/WCO.0000000000000837>.
- Chang, I.J., and Hahn, S.H. (2017). The genetics of Wilson disease. *Handb. Clin. Neurol.* 142, 19–34. <https://doi.org/10.1016/B978-0-444-63625-6.00003-3>.
- Bull, P.C., Thomas, G.R., Rommens, J.M., Forbes, J.R., and Cox, D.W. (1993). The Wilson disease gene is a putative copper transporting P-type ATPase similar to the Menkes gene. *Nat. Genet.* 5, 327–337. <https://doi.org/10.1038/ng1293-327>.
- Medici, V., and Weiss, K. (2017). Chapter 4 - Genetic and environmental modifiers of Wilson disease. In *Handbook of Clinical Neurology*, A. Członkowska and M.L. Schilsky, eds. (Elsevier), pp. 35–41.
- Boga, S., Ala, A., and Schilsky, M.L. (2017). Hepatic features of Wilson disease. *Handb. Clin. Neurol.* 142, 91–99. <https://doi.org/10.1016/B978-0-444-63625-6.00009-4>.
- Hellman, N.E., Kono, S., Mancini, G.M., Hoogeboom, A.J., de Jong, G.J., and Gitlin, J.D. (2002). Mechanisms of copper incorporation into human ceruloplasmin. *J. Biol. Chem.* 277, 46632–46638. <https://doi.org/10.1074/jbc.M206246200>.
- Pronicki, M. (2017). Wilson disease - liver pathology. *Handb. Clin. Neurol.* 142, 71–75. <https://doi.org/10.1016/B978-0-444-63625-6.00007-0>.
- Cobine, P.A., Moore, S.A., and Leary, S.C. (2021). Getting out what you put in: Copper in mitochondria and its impacts on human disease. *Biochim. Biophys. Acta Mol. Cell Res.* 1868, 118867. <https://doi.org/10.1016/j.bbamcr.2020.118867>.
- Zischka, H., and Einer, C. (2018). Mitochondrial copper homeostasis and its derailment in Wilson disease. *Int. J. Biochem. Cell Biol.* 102, 71–75. <https://doi.org/10.1016/j.biocel.2018.07.001>.
- Ekici, S., Turkarslan, S., Pawlik, G., Dancis, A., Baliga, N.S., Koch, H.G., Daldal, F.; Univ. Of Pennsylvania P.P.U.S., and Shuman, H.A. (2014). Intracytoplasmic copper homeostasis controls cytochrome c oxidase production. *mBio* 5, e01055-13. <https://doi.org/10.1128/mBio.01055-13>.
- Timón-Gómez, A., Nývltová, E., Abriata, L.A., Vila, A.J., Hosler, J., and Barrientos, A. (2018). Mitochondrial cytochrome c oxidase biogenesis: Recent developments. *Semin. Cell Dev. Biol.* 76, 163–178. <https://doi.org/10.1016/j.semcdb.2017.08.055>.
- Leary, S.C., Sasarman, F., Nishimura, T., and Shoubridge, E.A. (2009). Human SCO2 is required for the synthesis of CO II and as a thiol-disulphide oxidoreductase for SCO1. *Hum. Mol. Genet.* 18, 2230–2240. <https://doi.org/10.1093/hmg/ddp158>.
- Rebelo, A.P., Saade, D., Pereira, C.V., Farooq, A., Huff, T.C., Abreu, L., Moraes, C.T., Mnatsakanova, D., Mathews, K., Yang, H., et al. (2018). SCO2 mutations cause early-onset axonal Charcot-Marie-Tooth disease associated with cellular copper deficiency. *Brain* 141, 662–672. <https://doi.org/10.1093/brain/awx369>.
- Dai, C.Q., Luo, T.T., Luo, S.C., Wang, J.Q., Wang, S.M., Bai, Y.H., Yang, Y.L., and Wang, Y.Y. (2016). p53 and mitochondrial dysfunction: novel insight of neurodegenerative diseases. *J. Bioenerg. Biomembr.* 48, 337–347. <https://doi.org/10.1007/s10863-016-9669-5>.
- Tang, J.X., Thompson, K., Taylor, R.W., and Oláhová, M. (2020). Mitochondrial OXPHOS biogenesis: co-regulation of protein synthesis, import, and assembly Pathways. *Int. J. Mol. Sci.* 21, 3820. <https://doi.org/10.3390/ijms21113820>.
- Dhar, S.S., Ongwijitwat, S., and Wong-Riley, M.T.T. (2008). Nuclear respiratory factor 1 regulates all ten nuclear-encoded subunits of cytochrome c oxidase in neurons. *J. Biol. Chem.* 283, 3120–3129. <https://doi.org/10.1074/jbc.M707587200>.
- Tao, T., Sondalle, S.B., Shi, H., Zhu, S., Perez-Atayde, A.R., Peng, J., Baserga, S.J., and Look, A.T. (2017). The pre-rRNA processing factor DEF is rate limiting for the pathogenesis of MYCN-driven neuroblastoma. *Oncogene* 36, 3852–3867. <https://doi.org/10.1038/onc.2016.527>.
- Charette, J.M., and Baserga, S.J. (2010). The DEAD-box RNA helicase-like Utp25 is an SSU processome component. *RNA* 16, 2156–2169. <https://doi.org/10.1261/ma.2359810>.
- Tao, T., Shi, H., Guan, Y., Huang, D., Chen, Y., Lane, D.P., Chen, J., and Peng, J. (2013). Def defines a conserved nucleolar pathway that leads p53 to proteasome-independent degradation. *Cell Res.* 23, 620–634. <https://doi.org/10.1038/cr.2013.16>.
- Zhao, S., Huang, D., and Peng, J. (2021). Nucleolus-localized Def-CAPN3 protein degradation pathway and its role in cell cycle control and ribosome biogenesis. *J. Genet. Genomics* 48, 955–960. <https://doi.org/10.1016/j.jgg.2021.06.011>.
- Ono, Y., Ojima, K., Shinkai-Ouchi, F., Hata, S., and Sorimachi, H. (2016). An eccentric calpain, CAPN3/p94/calpain-3. *Biochimie* 122, 169–187. <https://doi.org/10.1016/j.biochi.2015.09.010>.
- Chen, F., Huang, D., Shi, H., Gao, C., Wang, Y., and Peng, J. (2020). Capn3 depletion causes Chk1 and Wee1 accumulation and disrupts synchronization of cell cycle reentry

- during liver regeneration after partial hepatectomy. *Cell Regen.* 9, 8. <https://doi.org/10.1186/s13619-020-00049-1>.
23. Guan, Y., Huang, D., Chen, F., Gao, C., Tao, T., Shi, H., Zhao, S., Liao, Z., Lo, L.J., Wang, Y., et al. (2016). Phosphorylation of Def regulates nucleolar p53 turnover and cell cycle progression through Def recruitment of Calpain3. *PLoS Biol.* 14, e1002555. <https://doi.org/10.1371/journal.pbio.1002555>.
 24. Ding, F., Huang, D., Wang, M., and Peng, J. (2022). An 86 amino acids motif in CAPN3 is essential for formation of the nucleolus-localized Def-CAPN3 complex. *Biochem. Biophys. Res. Co.* 623, 66–73. <https://doi.org/10.1016/j.bbrc.2022.06.032>.
 25. Chen, J., Ruan, H., Ng, S.M., Gao, C., Soo, H.M., Wu, W., Zhang, Z., Wen, Z., Lane, D.P., and Peng, J. (2005). Loss of function of def selectively up-regulates Delta13p53 expression to arrest expansion growth of digestive organs in zebrafish. *Gene Dev.* 19, 2900–2911. <https://doi.org/10.1101/gad.1366405>.
 26. Aryal, N.K., Wasylishen, A.R., Pant, V., Riley-Croce, M., and Lozano, G. (2017). Loss of digestive organ expansion factor (Diexf) reveals an essential role during murine embryonic development that is independent of p53. *Oncotarget* 8, 103996–104006. <https://doi.org/10.18632/oncotarget.22087>.
 27. Huang, W., Chen, F., Ma, Q., Xin, J., Li, J., Chen, J., Zhou, B., Chen, M., Li, J., and Peng, J. (2020). Ribosome biogenesis gene DEF/UTP25 is essential for liver homeostasis and regeneration. *Sci. China Life Sci.* 63, 1651–1664. <https://doi.org/10.1007/s11427-019-1635-2>.
 28. Boban, M., and Foisner, R. (2016). Degradation-mediated protein quality control at the inner nuclear membrane. *Nucleus* 7, 41–49. <https://doi.org/10.1080/19491034.2016.1139273>.
 29. Azkanaz, M., Rodríguez López, A., de Boer, B., Huiting, W., Angrand, P.O., Vellenga, E., Kampinga, H.H., Bergink, S., Martens, J.H., Schuringa, J.J., and van den Boom, V. (2019). Protein quality control in the nucleolus safeguards recovery of epigenetic regulators after heat shock. *Elife* 8, e45205. <https://doi.org/10.7554/eLife.45205>.
 30. Frottin, F., Schueder, F., Tiwary, S., Gupta, R., Körner, R., Schlichtharler, T., Cox, J., Jungmann, R., Hartl, F.U., and Hipp, M.S. (2019). The nucleolus functions as a phase-separated protein quality control compartment. *Science* 365, 342–347. <https://doi.org/10.1126/science.aaw9157>.
 31. Kaplan, J.H., and Maryon, E.B. (2016). How mammalian cells acquire copper: an essential but potentially toxic metal. *Biophys. J.* 110, 7–13. <https://doi.org/10.1016/j.bpj.2015.11.025>.
 32. Baird, L., and Yamamoto, M. (2020). The molecular mechanisms regulating the KEAP1-NRF2 pathway. *Mol. Cell Biol.* 40, e00099-20. <https://doi.org/10.1128/MCB.00099-20>.
 33. de Bie, P., van de Sluis, B., Burstein, E., van de Berghe, P.V.E., Muller, P., Berger, R., Gitlin, J.D., Wijmenga, C., and Klomp, L.W.J. (2007). Distinct Wilson's disease mutations in ATP7B are associated with enhanced binding to COMMD1 and reduced stability of ATP7B. *Gastroenterology* 133, 1316–1326. <https://doi.org/10.1053/j.gastro.2007.07.020>.
 34. Sharp, P.A. (2003). Ctr1 and its role in body copper homeostasis. *Int. J. Biochem. Cell Biol.* 35, 288–291. [https://doi.org/10.1016/s1357-2725\(02\)00134-6](https://doi.org/10.1016/s1357-2725(02)00134-6).
 35. Bustin, S.A., Beaulieu, J.F., Huggett, J., Jaggi, R., Kibenge, F.S.B., Olsvik, P.A., Penning, L.C., and Toegel, S. (2010). MIQE precis: Practical implementation of minimum standard guidelines for fluorescence-based quantitative real-time PCR experiments. *BMC Mol. Biol.* 11, 74. <https://doi.org/10.1186/1471-2199-11-74>.
 36. Liu, Z., Wang, M., Zhang, C., Zhou, S., and Ji, G. (2022). Molecular functions of ceruloplasmin in metabolic disease pathology. *Diabet. Metab. Synd. Ob.* 15, 695–711. <https://doi.org/10.2147/DMSO.S346648>.
 37. Czlonkowska, A., and Litwin, T. (2017). Wilson disease - currently used anticopper therapy. *Handb. Clin. Neurol.* 142, 181–191. <https://doi.org/10.1016/B978-0-444-63625-6.00015-X>.
 38. Gauthier, L., Charbonnier, P., Chevallet, M., Delangle, P., Texier, I., Gateau, C., and Deniaud, A. (2021). Development, formulation, and cellular mechanism of a lipophilic copper chelator for the treatment of Wilson's disease. *Int. J. Pharm.* 609, 121193. <https://doi.org/10.1016/j.ijpharm.2021.121193>.
 39. Huster, D., and Lutsenko, S. (2007). Wilson disease: not just a copper disorder. Analysis of a Wilson disease model demonstrates the link between copper and lipid metabolism. *Mol. Biosyst.* 3, 816–824. <https://doi.org/10.1039/b711118p>.
 40. Huster, D., Purnat, T.D., Burkhead, J.L., Ralle, M., Fiehn, O., Stuckert, F., Olson, N.E., Teupser, D., and Lutsenko, S. (2007). High copper selectively alters lipid metabolism and cell cycle machinery in the mouse model of Wilson disease. *J. Biol. Chem.* 282, 8343–8355. <https://doi.org/10.1074/jbc.M607496200>.
 41. Huo, Y., Ma, F., Li, L., Li, Y., Zhong, G., Liao, J., Han, Q., Li, Y., Pan, J., Hu, L., et al. (2023). Effect of copper exposure on the cholesterol metabolism in broiler liver. *Biol. Trace Elem. Res.* <https://doi.org/10.1007/s12011-023-03609-z>.
 42. He, L., Pu, W., Liu, X., Zhang, Z., Han, M., Li, Y., Huang, X., Han, X., Li, Y., Liu, K., et al. (2021). Proliferation tracing reveals regional hepatocyte generation in liver homeostasis and repair. *Science* 371, eabc4346. <https://doi.org/10.1126/science.abc4346>.
 43. Wang, S., Yang, J., You, L., Dai, M., and Zhao, Y. (2020). GSTM3 function and polymorphism in cancer: emerging but promising. *Cancer Manag. Res.* 12, 10377–10388. <https://doi.org/10.2147/CMAR.S272467>.
 44. Matoba, S., Kang, J.G., Patino, W.D., Wragg, A., Boehm, M., Gavrilova, O., Hurley, P.J., Bunz, F., and Hwang, P.M. (2006). p53 regulates mitochondrial respiration. *Science* 312, 1650–1653. <https://doi.org/10.1126/science.1126863>.
 45. Zhang, X.D., Qin, Z.H., and Wang, J. (2010). The role of p53 in cell metabolism. *Acta Pharmacol. Sin.* 31, 1208–1212. <https://doi.org/10.1038/aps.2010.151>.
 46. Stiburek, L., Vesela, K., Hansikova, H., Hulkova, H., and Zeman, J. (2009). Loss of function of Sco1 and its interaction with cytochrome oxidase. *Am. J. Physiol. Cell Physiol.* 296, C1218–C1226. <https://doi.org/10.1152/ajpcell.00564.2008>.
 47. Leary, S.C., Cobine, P.A., Kaufman, B.A., Guercin, G.H., Mattman, A., Palaty, J., Lockitch, G., Winge, D.R., Rustin, P., Horvath, R., and Shoubridge, E.A. (2007). The human cytochrome c oxidase assembly factors SCO1 and SCO2 have regulatory roles in the maintenance of cellular copper homeostasis. *Cell Metabol.* 5, 9–20. <https://doi.org/10.1016/j.cmet.2006.12.001>.
 48. Pietrancosta, N., Moumen, A., Dono, R., Lingor, P., Planchamp, V., Lamballe, F., Bähr, M., Kraus, J.L., and Maina, F. (2006). Iminotetrahydro-benzothiazole derivatives as p53 inhibitors: discovery of a highly potent in vivo inhibitor and its action mechanism. *J. Med. Chem.* 49, 3645–3652. <https://doi.org/10.1021/jm060318n>.
 49. Chen, J., Jiang, Y., Shi, H., Peng, Y., Fan, X., and Li, C. (2020). The molecular mechanisms of copper metabolism and its roles in human diseases. *Pflügers Archiv* 472, 1415–1429. <https://doi.org/10.1007/s00424-020-02412-2>.
 50. Boulet, A., Vest, K.E., Maynard, M.K., Gammon, M.G., Russell, A.C., Mathews, A.T., Cole, S.E., Zhu, X., Phillips, C.B., Kwong, J.Q., et al. (2018). The mammalian phosphate carrier SLC25A3 is a mitochondrial copper transporter required for cytochrome c oxidase biogenesis. *J. Biol. Chem.* 293, 1887–1896. <https://doi.org/10.1074/jbc.RA117.000265>.
 51. Vest, K.E., Leary, S.C., Winge, D.R., and Cobine, P.A. (2013). Copper import into the mitochondrial matrix in *Saccharomyces cerevisiae* is mediated by Pic2, a mitochondrial carrier family protein. *J. Biol. Chem.* 288, 23884–23892. <https://doi.org/10.1074/jbc.M113.470674>.
 52. Zhao, S., Chen, Y., Chen, F., Huang, D., Shi, H., Lo, L.J., Chen, J., and Peng, J. (2019). Sas10 controls ribosome biogenesis by stabilizing Mpp10 and delivering the Mpp10-Imp3-Imp4 complex to nucleolus. *Nucleic Acids Res.* 47, 2996–3012. <https://doi.org/10.1093/nar/gkz105>.
 53. Qi, Z., He, J., Su, Y., He, Q., Liu, J., Yu, L., Al-Attas, O., Hussain, T., Ding, S., Ji, L., and

- Qian, M. (2011). Physical exercise regulates p53 activity targeting SCO2 and increases mitochondrial COX biogenesis in cardiac muscle with age. *PLoS One* 6, e21140. <https://doi.org/10.1371/journal.pone.0021140>.
54. Polishchuk, E.V., Merolla, A., Lichtmanegger, J., Romano, A., Indrieri, A., Ilyechova, E.Y., Concilli, M., De Cegli, R., Crispino, R., Mariniello, M., et al. (2019). Activation of autophagy, observed in liver tissues from patients with Wilson disease and from ATP7B-deficient animals, protects hepatocytes from copper-induced apoptosis. *Gastroenterology* 156, 1173–1189.e5. <https://doi.org/10.1053/j.gastro.2018.11.032>.
55. Han, X., Wang, R., Zhou, Y., Fei, L., Sun, H., Lai, S., Saadatpour, A., Zhou, Z., Chen, H., Ye, F., et al. (2018). Mapping the mouse cell atlas by microwell-seq. *Cell* 172, 1091–1107.e17. <https://doi.org/10.1016/j.cell.2018.02.001>.
56. Gao, Y., Jin, Q., Gao, C., Chen, Y., Sun, Z., Guo, G., and Peng, J. (2022). Unraveling differential transcriptomes and cell types in zebrafish larvae intestine and liver. *Cells* 11, 3290. <https://doi.org/10.3390/cells11203290>.
57. Jin, Q., Gao, Y., Shuai, S., Chen, Y., Wang, K., Chen, J., Peng, J., and Gao, C. (2022). Cdx1b protects intestinal cell fate by repressing signaling networks for liver specification. *J. Genet. Genomics* 49, 1101–1113. <https://doi.org/10.1016/j.jgg.2022.11.006>.
58. Zhu, Y., Wang, Y., Tao, B., Han, J., Chen, H., Zhu, Q., Huang, L., He, Y., Hong, J., Li, Y., et al. (2022). Nucleolar GTPase Bms1 displaces Ttf1 from RFB-sites to balance progression of rDNA transcription and replication. *J. Mol. Cell Biol.* 13, 902–917. <https://doi.org/10.1093/jmcb/mjab074>.

STAR★METHODS

KEY RESOURCES TABLE

REAGENT or RESOURCE	SOURCE	IDENTIFIER
Antibodies		
rabbit-anti-ATOX1 polyclonal	Proteintech	Cat#22641-1-AP; RRID: AB_2879139
rabbit-anti-ATP7B polyclonal	Proteintech	Cat#19786-1-AP; RRID: AB_2878607
rabbit-anti-ATP7B polyclonal	Affinity	Cat# DF3166; RRID:AB_2835542
rabbit-anti-CP polyclonal	Proteintech	Cat#21131-1-AP; RRID: AB_2878815
rabbit-anti-ACTIN polyclonal	ABclonal	Cat#AC026;RRID: AB_2768234
rabbit-anti-CTR1 polyclonal	ABclonal	Cat#A10109;RRID: AB_2757632
rabbit-anti-NRF1 polyclonal	ABclonal	Cat#A5547;RRID: AB_2766328
rabbit-anti-SCO2 polyclonal	ABclonal	Cat#A7051;RRID: AB_2767606
mouse-anti-TUBULIN polyclonal	ABclonal	Cat#AC021;RRID: AB_2773004
rabbit-anti-COX1 polyclonal	Abcam	Cat#ab203912;RRID: AB_2801537
mouse-anti-FIB polyclonal	Abcam	Cat#ab4566;RRID: AB_304523
mouse-anti-P53 polyclonal	Santa Cruz	Cat#sc-126;RRID: AB_628082
rabbit-anti-LAMINB polyclonal	Abcam	Cat#ab133741;RRID:AB_2731736
rabbit-anti-LAMP1 polyclonal	ABclonal	Cat#A16894;RRID:AB_2770145
rabbit-anti-COX17 polyclonal	Huabio	Cat#ER63100
guinea pig-anti-mDEF polyclonal	ABClonal	N/A
rabbit-anti-CAPN3 polyclonal	Huabio	N/A
Chemicals, peptides, and recombinant proteins		
meso-2,3-Dimercaptosuccinic acid (DMSA)	Sigma-Aldrich	Cat#304-55-2
Pifithrin- α (PTF)	MCE	Cat#60477-38-5
collagenase IV	Gibco	Cat#9001-12-1
EGTA	Thermo Scientific	Cat#J60767
HEPEs,free acid	Beyotime	Cat#ST092
Glycerol	Sangon Biotech	Cat#A600232-0500
β -Mercaptoethanol	Febio science	Cat#FD2120
TRIpure Reagent	Aidlab	Cat#RN0102
DNaseI	Thermo Scientific	Cat#EN0521
M-MLV Reverse Transcriptase	Invitrogen	Cat#28025-021
AceQq SYBR Green Master Mix	Vazyme	Cat#Q111-02
Alexa Fluor-647	Abcam	Cat#ab150115
Alexa Fluor-488	Abcam	Cat#ab150077
DAPI	Abcam	Cat#ab285390
cOmplete Protease Inhibitor Cocktail tablets	Roche	Cat#04693159001
PMSF	Beyotime Biotechnology	Cat#329-98-6
D-hanks	Meilunbio	Cat#MA0039
RIPA	Beyotime Biotechnology	Cat#P0013B
Critical commercial assays		
Reactive Oxygen Species Assay Kit	Beyotime Biotechnology	Cat#S0033S
Cell Mitochondria Isolation Kit	Beyotime Biotechnology	Cat#C3601

(Continued on next page)

Continued

REAGENT or RESOURCE	SOURCE	IDENTIFIER
<i>Deposited data</i>		
Transcriptome of mouse liver	This paper	BioProject ID:PRJNA923397
Transcriptome of single cell	This paper	BioProject ID: PRJNA923397
Raw data	This paper	https://doi.org/10.17632/xcs56hxx6x.1
<i>Experimental models: Organisms/strains</i>		
Mouse : WT : C57BL/6JGpt ^{WT/WT}	Gem Pharmatech	N/A
Mouse : mDef ^{loxP/loxP} : C57BL/6JGpt ^{fl/fl}	Gem Pharmatech	N/A
Mouse : Alb : Cre : C57BL/6JGpt ^{Alb:Cre}	Model Animal Research Center of Nanjing University	N/A
<i>Oligonucleotides</i>		
CCTGGTGATGTCCGACCTG	This paper	<i>Cdkn1a_Forward</i>
CCATGAGGCATCGCAATC	This paper	<i>Cdkn1a_Reverse</i>
TGTCTGTGTCTACCGAGGGTG	This paper	<i>Mdm2_Forward</i>
TCCAACGGACTTTAAACAATTCA	This paper	<i>Mdm2_Reverse</i>
TGAAGACAGGGGCCTTTTTG	This paper	<i>Bax_Forward</i>
AATTCGCCGGAGACACTCG	This paper	<i>Bax_Reverse</i>
AGCTCTCTCAGTTCAAACCCC	This paper	<i>Sco2_Forward</i>
GCAGTCTAGTTCTTAGCCCAG	This paper	<i>Sco2_Reverse</i>
GAGCAGCTCCTTTGCTCTC	This paper	<i>Sco2_Forward_2</i>
TCTTTGGATTAGCGGACAGG	This paper	<i>Sco2_Reverse_2</i>
CTCCGTGGACATGACCTGTG	This paper	<i>Atox1_Forward</i>
GTTGAACTCCACTCCTCCAG	This paper	<i>Atox1_Reverse</i>
CCATTGCTACTCAGTTGGC	This paper	<i>Atp7b_Forward</i>
TGGCCACGACGTCCAATAAG	This paper	<i>Atp7b_Reverse</i>
CTCCTCACAGCAAGCCTCC	This paper	<i>Cp_Forward</i>
TGGGTCCCATTTCTTTGGGG	This paper	<i>Cp_Reverse</i>
GGGCTTACCCTGTGAAGACTTT	This paper	<i>Ctr1_Forward</i>
GTGGTGAGGTGGCATGGTAA	This paper	<i>Ctr1_Reverse</i>
AGGTCGGTGTGAACGGATTTG	This paper	<i>Gapdh_Forward</i>
TGTAGACCATGTAGTTGAGGTCA	This paper	<i>Gapdh_Reverse</i>
GTGACGTTGACATCCGTAAAGA	This paper	<i>Actin_Forward</i>
GCCGGACTCATCGTACTCC	This paper	<i>Actin_Reverse</i>
GCAGGCATCCATCGCCAGTCCA	This paper	<i>18S_Forward</i>
CCGTAGCTCGATGCTAGCCCTGG	This paper	<i>18S_Reverse</i>
CACGGGACTCAGCAGTGATA	This paper	<i>mt-Rnr1_Forward</i>
GTTGACACGTTTTACGCCGA	This paper	<i>mt-Rnr1_Reverse</i>
CCGCAAGGGAAAGATGAAAGAC	This paper	<i>mt-Rnr2_Forward</i>
TCGTTTGGTTTCGGGGTTTC	This paper	<i>mt-Rnr2_Reverse</i>
GCCAGCCTCTCCTGATTTAGTGT	This paper	<i>Hk2_Forward</i>
GGGAACACAAAAGACCTCTTCTGG	This paper	<i>Hk2_Reverse</i>
CCAGGTTTGATGGGAGGTAG	This paper	<i>Def-loxp_Forward</i>
CTGAGGAGTAACTAACGACC	This paper	<i>Def-loxp_Reverse</i>
ATTTGCCTGCATTACCGGTC	This paper	<i>Cre_Forward</i>
ATCAACGTTTTCTTTCCGG	This paper	<i>Cre_Reverse</i>

(Continued on next page)

Continued

REAGENT or RESOURCE	SOURCE	IDENTIFIER
AGGGGAACAGCTCCAGATGGCA	This paper	<i>Alb-Cre_Forward</i>
ACCGGCAAACGGACAGAAGCAT	This paper	<i>Alb-Cre_Reverse</i>

Software and algorithms

fastp	Version 0.23.2	https://github.com/OpenGene/fastp
hisat2	Version 2.2.1	https://github.com/DaehwanKimLab/hisat2
STAR	Version 2.5.2	https://github.com/alexdobin/STAR
dropEst	Version 0.8.6	https://github.com/kharchenkolab/dropEst
Subread	Version 2.0.3	https://github.com/ShiLab-Bioinformatics/subread
DESeq2	Version 1.38.2	https://bioconductor.org/packages/release/bioc/html/DESeq2.html
biomaRt	Version 2.54.0	https://bioconductor.org/packages/release/bioc/html/biomaRt.html
Seurat	Version 4.2.0	http://satijalab.org/seurat
R package	The R Foundation	https://www.r-project.org

RESOURCE AVAILABILITY**Lead contact**

Further information and requests for resources or reagents should be directed to the lead contact, Jinrong Peng (pengjr@zju.edu.cn).

Materials availability

All unique/stable reagents generated in this study are available from the [lead contact](#) with a completed Materials Transfer Agreement.

Data and code availability

- All related raw data have been submitted to Mendeley Data (<https://data.mendeley.com/>, ID number: <https://doi.org/10.17632/xcs56hxx6x.1>). Raw bulk and single RNA-sequencing data were deposited in the NCBI Sequence Read Archive (NCBI: Submission ID: SUB12531174; BioProject ID: PRJNA923397). All data present in this study will be shared by the [lead contact](#) upon request.
- This paper does not report original code.
- Any additional information required to reanalyze the data reported in this paper is available from the [lead contact](#) upon request.

EXPERIMENTAL MODEL AND STUDY PARTICIPANT DETAILS**Mouse stains**

All animal procedures were performed in full accordance with the "Guide for the Care and Use of Laboratory Animals" issued by the Animal Ethics Committee in Zhejiang University with permission (AP CODE: ZJU20220068). Mice were housed in a temperature-controlled environment under a 12 hour (hr) light:dark cycle with free access to water and food. Mouse C57BL/6 strain was used as the wild type (WT) animal in all experiments. The *mDef* hepatocyte conditional knockout mice (*mDef^{loxp/loxp},Alb:Cre*) (designated as *mDef-CKO* thereafter) was generated by crossing the *mDef^{loxp/loxp}* homozygous mice with the *Alb:Cre* as described previously.²⁷ *Alb:Cre* mice were purchased from Model Animal Research Center of Nanjing University. *mDef* hepatocyte conditional knockout male mice were also generated by injecting a single dose (1×10^{11} virus titer) of the AAV8.TBG.Cre virus (for expressing *Cre* in the hepatocytes specifically) into the caudal vein of the *mDef^{loxp/loxp}* homozygous mice at around 2 months postnatal. The 9-10-week-old male mice were used to isolate mitochondrion and directly detect metal ion in liver. The 9-10-week-old male mice liver were used for TEM, bulk RNA-seq and sc-RNA-seq experiment. Mice were genotyped using gene specific primers listed in the [key resources table](#).

METHOD DETAILS

Ryanodine staining

Liver tissue was fixed with 4% PFA and sectioned for Ryanodine staining following the supplier's instruction. Stained samples were photographed under a microscopic scanner (KF-PRO-120, KFBIO).

Drug treatment

To investigate the mitochondrial damage caused by an excessive load of Cu, normal chow diet fed mice were allowed to drink water supplemented with Cu chelating agent meso-2,3-Dimercaptosuccinic acid (DMSA) or CuSO₄. To investigate the role of p53 in Cu accumulation, mice were injected intraperitoneally with single dose of 2.2 mg/kg of Pifithrin- α (PTF) (p53 inhibitor) every three days for a duration of 45 days.

Transmission electron microscopy (TEM)

For TEM, the sample was first fixed with 2.5% glutaraldehyde in phosphate buffer (0.1M, pH7.0) and washed in the phosphate buffer; then postfixed with 1% OsO₄ in phosphate buffer and washed in the phosphate buffer. After that, the sample was dehydrated by a graded series of ethanol (30%, 50%, 70%, 80%) and a graded series of acetone (90%, 95%, 100%). The specimen was placed in the mixture of absolute acetone and the Spurr resin (Tedpella) before embedding. The specimen was sectioned in LEICA EM UC7 ultratome and sections were stained by uranyl acetate and alkaline lead citrate, respectively, and were observed using a Hitachi Model H-7650 TEM.

Liver tissue harvesting and primary hepatocyte culture

Male mice were anesthetized with pentobarbital sodium and the liver was perfused twice, first with EGTA-D-Hanks solution (clearance of blood cells and immune cells) for 5-7 minutes (min) and second with collagenase IV-D-Hanks solution (for *in situ* digestion of liver) for 6-8 min. The liver tissue was then dissected after abdomen operation using a surgical scissors and dispersed by removing the epidermal layer to produce primary hepatocytes. Primary hepatocytes were cultured in the William's E medium.

Mitochondria isolation

Mitochondria were isolated from the perfused liver tissue using a cell mitochondrial kit (C3601, Beyotime, Shanghai, China) according to the manufacturer's instructions. Isolated hepatocytes were incubated in the cell lysis buffer (250mM of sucrose; 1mM of DTT; 10mM of KCl; 1mM of EDTA; 1mM of EGTA; 1.5mM of MgCl₂; phenylmethylsulfonyl fluoride; 20mM of HEPEs, pH 7.4) at 4°C and homogenized with a glass homogenizer. The cell lysate was centrifuged at 800 \times g for 10 min to remove any unbroken cells, and the supernatant was further centrifuged at 15,000 \times g for 10 min at 4°C. The resulting supernatant contained the cytoplasmic fraction and the pellet contained the mitochondrial fraction.

Protein analysis

Total liver protein was extracted from the dissected raw liver tissue on ice throughout. 0.1g/ml RIPA lysis buffer (Beyotime Biotechnology) and steel beads were added to the tissue. The mixture was grounded with tissue grinder. After incubation for 10 min on ice the lysate was centrifuged at 12,000 rpm for 15 min. The supernatant was used as protein samples. After denaturation with the SDS lysis buffer (10% Glycerol, 5% β -Mercaptoethanol, 3.5% SDS, 63 mM Tris-HCl in RO water) the protein samples were subjected to an SDS PAGE. After electrophoresis, proteins were transferred to a PVDF membrane (TRANS BLOT® SD SEMI-DRY TRANSFER CELL, Bio-Rad Cat. No.170-3940). PVDF membrane was used for western blot analysis using specific antibodies according to the standard protocol provided by the manufacturer. After staining with the super-sensitive substrate (Trans Cat.No.DW101-02, Beijing, China) or normal substrate (Sunkyo Cat.No.61804, Beijing, China), the positive signals were acquired by an imager (ChemiScope 3400, CLiNX). The mDEF and CAPN3 antibodies were generated by ABClonal (Wuhan, China) and Huabio (Hangzhou, China), respectively. Antibodies against ATOX1 (22641-1-AP), ATP7B (19786-1-AP), CP (21131-1-AP) were purchased from Proteintech (Chicago, USA), ACTIN (ac026), CTR1 (A10109), NRF1 (A5547), SCO2 (A7051), TUBULIN (ac021) from ABClonal, COX1 (ab203912), FIB (ab4566) from Abcam (Cambridge, England) and p53 (Do-1) from Santa Cruz (CA, USA).

Quantitative real-time PCR (qRT-PCR)

Total RNA was extracted from the dissected raw liver tissue using TRIpureReagent (Aidlab, RN0102) according to the manufacturer's instructions. In brief, 1 ml Trizol and steel beads were added into 0.05 g fresh

liver tissue. The mixture was grounded into homogenate, and placed at room temperature for 5min. After centrifuging for 10 min at 4°C with 10000 ×g, the supernatant was taken and 200 uL chloroform was added in. The mixture was shaken violently for 15 seconds and placed at room temperature for 3 min before being centrifuged at 4 °C at 10,000 ×g for 15 min. The supernatant was taken and 500 uL isopropanol was added and mixed gently. The mixture was placed at room temperature for 10 min before centrifugation at 4°C at 12000 ×g for 10 min. The supernatant was removed and the RNA pellet was washed with precooled 75% ethanol twice. After drying ethanol at 42°C, DEPC water was added to dissolve the RNA.

For qRT-PCR, total RNA was treated with DNaseI (Thermo Scientific, EN0521) prior to reverse transcription. Synthesis of cDNA was performed using 1 µg total RNA from each sample using M-MLV Reverse Transcriptase (Invitrogen, 28025-021). qRT-PCR was performed on a CFX96 Real-Time System (Bio-Rad, C1000 ThermalCycler) with AceQq PCR SYBR Green Master Mix (Vazyme, Q111-02) according to the manufacturer's instructions and analyzed on a BioRad CFX96 apparatus (Bio-Rad). Gene specific primers were listed in the [key resources table](#). Data analysis was performed according to MIQE-precise guidelines.³⁵ qPCR normalisation with reference genes were listed in [Table S8](#).

Bulk RNA-seq

For bulk RNA-seq, total RNA was extracted from the dissected WT and *Def*-CKO mice liver, respectively, and the quality was assessed on Bioanalyzer 2100 system (Agilent Technologies, CA, USA). The procedures for the library construction included mRNA purification by poly-T oligo-attached magnetic beads, RNA fragmentation, reverse transcription using random hexamer primers and M-MuLV reverse transcriptase, followed by RNA degradation with RNase H treatment, second strand cDNA synthesis with DNA Polymerase I, blunt ends repair, 3' ends adenylation, adaptor ligation, 370~420bp cDNA fragments selection using the AMPure XP system (Beckman Coulter, Beverly, USA). Library was amplified with Phusion High-Fidelity DNA polymerase and quality assessment. Samples were sequenced on Illumina Novaseq platform to produce 150 bp paired-end reads. The sequencing data were deposited in the NCBI Sequence Read Archive (submission ID: SUB12531174; BioProject ID:PRJNA923397). Clean reads were mapped to the mouse genome (GRCm39) using the software Hisat2 v2.0.5 with default parameters.

Single cell RNA sequencing (scRNA-seq)

The scRNA-seq was performed using home-made microwell-seq platform.⁵⁵⁻⁵⁷ WT and *Def*-CKO samples were, respectively, perfused with Solution I (0.75 g/L EGTA D-Hank's PH7.2-7.4) for 5-7 min first and then digested with Solution II (50 mg/L collagenase type IV-D-Hank's) for 6-8 min. The full-length cDNA was fragmented by a transposase from TruePrep DNA Library Prep Kit V2 for Illumina (Vazyme), which carries two insertion sequences. Then, AMPure XP beads were used to purify this library. Finally, cDNA library about 400 to 700 bp were sequenced on an Illumina Hiseq system.⁵⁵⁻⁵⁷ Reads alignment and generation of the gene-barcode matrices from FASTQ files including Read 1 and Read 2 were performed with dropEst (v0.8.5). Elbow plot using Seurat was showed in [Figure S8](#). Finally, 10 optimal principal components (PCs) were determined for clustering and following data analysis.⁵⁵⁻⁵⁷ Data were filtered according to the following criteria: nFeature_RNA (unique genes) between 200-2500, percent.mt (mitochondrial gene percentage) <10, dimensions 1:10 and resolution 0.3. The scRNA-seq and bulked RNA-seq data were deposited together in the NCBI Sequence Read Archive (submission ID: SUB12531174; BioProject ID: PRJNA923397).

Immunofluorescence staining

Immunofluorescence staining of the cultured cells was as previously described.⁵⁸ The cell slides were washed twice with PBS after media removal and fixed using 4% PFA for 15 mins, then permeabilized in 0.1% PBS Triton and blocked(5% goat serum in 0.1% PBS Triton) for 30 mins at room temperature. After overnight incubation with the first antibody in the hybridization buffer (PBS plus 0.5%BSA and 0.2% Triton X-100), fluorescence (Alexa Fluor-647 and Alexa Fluor-488) conjugated second antibody was added and incubated for 60 min. After addition of DAPI, the staining signals were acquired under a laser confocal microscope (Olympus FV1000).

Nuclei isolation

Nucleus were isolated from the perfused liver tissue. First hepatocytes were incubated in Buffer A (10 mM 4-(2-hydroxyethyl)-1-piperazineethanesulfonic acid (HEPES), pH 7.9, 10 mM KCl, 1.5 mM MgCl₂ and 0.5 mM

DTT) for 30 mins. The sample was ground 20-35 times with a grinder until 90% of the hepatocytes nuclei were released. After centrifugation at 3500g and 4°C for 10 min, the precipitates were resuspended in S1 (0.5 M sucrose, 3 mM MgCl₂). Resuspended liquid was layered onto the S2 buffer (1 M sucrose, 3 mM MgCl₂) and centrifuged at 1800g for 10 min. The pellet was collected as the nuclear fraction and the supernatant as the cytoplasmic fraction.

Bile collection

Male mice were anesthetized with pentobarbital sodium. After laparotomy, insulin needles were used for the aspiration of the bile. The extracted bile is frozen in liquid nitrogen until use.

Liver total cholesterol detection

Mice liver TCHO was detected by WuHan PINUOFEI Biological Technology. Mouse liver was ground with addition of nine volumes of homogenization medium, and then the grinding mixture was centrifuged for 10 minutes (3000-4000g), and the supernatant was used for TCHO detection. TCHO was detected by Mouse TCHO test kit (C-63529 and the TCHO content was normalized against the BSA level in the sample.

QUANTIFICATION AND STATISTICAL ANALYSIS

Hepatic Cu quantification

Raw liver tissue was harvested for quantifying metal ions including Li, Mg, Al, Cr, Mn, Fe, Co, Cu, Zn, Ge, Cd, Ba, Tl, Pb. Hepatocytes and mitochondria were isolated from the perfused liver tissue, respectively, for quantifying Cu, Fe and Mg. Metal ions in the liver, hepatocytes and mitochondria were detected using the inductively coupled plasma mass spectrometry (ICP-MS) method. In brief, samples were digested with 100% nitric acid, and were then subjected to analysis by a Thermo iCAP RQ instrument. Data were analyzed by the QTEGRA system.

Differential gene-expression analysis of RNA sequencing data

For the bulk RNA-seq, after mapping the clean reads to the mouse genome (GRCm39) using the software Hisat2 v2.0.5 with default parameters, transcript levels were obtained for each gene and the differentially expressed genes (DEGs) was determined with DESeq2 (v1.28.1). Gene ontology (GO) set overrepresentation analysis of the DEGs was conducted with the ClusterProfiler (v3.16.1) software tool.

scRNA-seq data analysis

For the scRNA-seq, after filtering the sequence data, qualified gene reads in each cell were analyzed using the R package Seurat (v4.0, Vienna, Austria) (<https://mran.microsoft.com/snapshot/2020-05-30/bin/windows/base/>) according to the instruction.

Detection of intracellular ROS

Intracellular ROS was detected by means of an oxidation-sensitive fluorescent probe 2',7'-dichlorofluorescein-diacetate (DCFH-DA). DCFH-DA was deacetylated intracellularly by nonspecific esterase, which was further oxidized by ROS to the fluorescent compound 2,7-dichlorofluorescein (DCF). DCF fluorescence was detected by laser confocal microscope (Olympus FV1000). Signal intensity was quantified the using ImageJ software package.

Statistical analysis

Unless stated otherwise, all parameters were tested using unpaired two-tailed Student's t-test. Significant *p*-value in all statistical analyses was obtained using GraphPad Prism 9 (GraphPad Software). A *p*-value below 0.05 was considered to be statistically significant. Unless stated otherwise, the experiments were not randomized and investigators were not blinded to allocation during experiments.